Will COTS RF Front-Ends Really Cope With 5G Requirements at mmWave?

RODOLFO GOMES[1,2], (Student Member, IEEE), LUÍS SISMEIRO[3,4], (Student Member, IEEE), CARLOS RIBEIRO[2,3], TELMO R. FERNANDES [1,2,3], (Senior Member, IEEE), MANUEL GARCIA SANCHÉZ [4], (Senior Member, IEEE), AKRAM HAMMOUDEH[1], AND RAFAEL F. S. CALDEIRINHA [1,2,3], (Senior Member, IEEE)

[1]School of Engineering, University of South Wales, Pontypridd CF37 1DL, U.K.
[2]Instituto de Telecomunicações, 2411-901 Leiria, Portugal
[3]Polytechnic Institute of Leiria, 2411-901 Leiria, Portugal
[4]Department Teoría do Sinal e Comunicacions, Universidade de Vigo, 36310 Vigo, Spain

Corresponding author: Rafael F. S. Caldeirinha (rafael.caldeirinha@ipleiria.pt)

ABSTRACT In this paper, the real-time over-the-air multi-gigabit wideband wireless orthogonal frequency division multiplexing (OFDM) system performance, using two distinct radio frequency (RF) front-ends designed for the millimetre frequency band (mmWave), is evaluated. A thorough comparative analysis between 60-GHz cutting-edge commercial off-the-shelf and reference RF front-ends, taking into account their intrinsic RF impairments and their impact on the overall system performance degradation, is presented. With this, it is possible to verify whether system on chip technology for RF circuits is ready for 5G systems. Due to the large available bandwidth, the mmWave band is very attractive for future 5G wireless communication systems, which might provide transmission data rates over 10 Gb/s and network latency below 1 ms. However, non-linearities of RF front-ends, at these frequencies, severely affect the performance of transmission schemes. In fact, this is the main cause for performance degradation on OFDM systems. It causes significant limitation on both maximum spectral efficiency and data rate of the wireless communication link. Therefore, the OFDM performance degradation due to the non-linearities from both analogue stages of upconversion/downconversion is evaluated considering important key performance indicators for quality of service in digital communications considering 4-, 16-, 64- and 256-quadrature amplitude modulation. Furthermore, based on the results obtained from appropriate RF measurements, a practical EVM link budget formulation for mmWave systems, which takes into account both PA and PN impairment effects, is proposed.

INDEX TERMS 5G, OFDM, SDR, mmWave, RF impairments, testbeds, RF front-ends.

I. INTRODUCTION

Mobile communications has become one of the utmost important enterprises in modern history [1]. In fact, after twenty years after the deployment of the second generation (2G) standard for digital mobile phones, radio communications have constantly been evolving. For example, currently Long Term Evolution Advanced (LTE-Advanced) standard is the fourth generation (4G) of mobile communications, where data-rates of 3 Gbps are provided in downlink scenarios [2]. This has lead to breakthroughs in semiconductors processes, and also to worldwide agreements between national frequency spectrum regulators [3]. Furthermore, it is expected that by 2021, the number of mobile devices will reach 3.5 per capita [4]. In this context, and to anticipate increasing mobile traffic congestion, a fifth wireless communication generation (5G) is intended to be released by 2020 [1], [3], [5]. This standard will not only be focused in the improvement of Quality of Service (QoS) in telecommunications, but also in assisting users with daily routine life interactions [6], providing

IEEE Access

R. Gomes *et al.*: Will COTS RF Front-Ends Really Cope With 5G Requirements at mmWave?

new possibilities such as: autonomous vehicles [7], video streaming [3], and virtual reality [8]. Therefore, massive inter-connection of users and devices, are merging the key applications in a globalised service including: Internet of Things (IoT), Machine-to-Machine (M2M) communication, Gigabit wireless connectivity, Tactile Internet, Centralized Radio Access Networks (CRAN) and Heterogeneous Networks (Hetnets) [9]–[12]. These applications will thus require 5G to be "flexible, scalable, robust, reliable, and efficient in terms of energy and spectrum" [13], capable of providing such wide specifications with low latencies (< 1 ms), and high data-rates (≥ 10 Gbps) [10], [11], [13].

Millimetre wave frequencies, and small Radio Frequency (RF) cell coverage, will therefore be considered [6] as key booster technologies towards the first 5G deployment. On one hand, Millimetre frequency band (mmWave) spectrum enables the usage of higher signal bandwidth in comparison with the sub-6 GHz spectrum band [3], [7], [14], and consequently enables higher data communication speeds. On the other hand, such signals are characterized by higher path losses [15], which limit the maximum range of coverage within a network cell. Nevertheless, this might be overcome through the implementation of small RF coverage cells, which might also reduce signal congestion, since fewer users will be assigned per cell. In fact, the most critical drawback, in a small cell scenario, when utilizing this band, is the presence of the non-idealities in the RF components, causing significant distortion of the transmitted signals. Therefore, system design becomes even more challenging when compared with the conventional sub-6 GHz band systems [16]. For example, the upconversion of baseband signals at the transmitter (TX) and their down conversion back to baseband at the receiver (RX), causes the RF front-ends to induce several critical non-linearities, affecting both transmitted and received radio signals. This includes Phase-Noise (PN), In-phase and Quadrature (IQ) imbalances and Power Amplifier (PA) non-linear distortions [16], and should be taken into account in radio system design and link quality prediction.

The 60 GHz band, has for a few decades been considered as an alternative to lower frequency signals [17], [18] due to its large and worldwide unlicensed bandwidth availability [3], [7], [8]. However, its utilization in previous generations of mobile communications was impractical due to large costs associated with RF chip-set manufacture [3]. Recent evolution in integrated circuits technology and design techniques [19], led to cost effective implementations of such chips. Additionally, the inherent small form factor, enables a massive number of antennas to be placed on chip at both ends of the radio link, and therefore massive Multiple-Input Multiple-Output (MIMO) solutions for 5G. Furthermore, the development of mmWave frequency standards such as IEEE 802.11ad (also known as WiGig) [20], IEEE 802.15.3c [21] and IEEE 802.11ay [22], demonstrates that 60 GHz band technology is mature enough to reach the open market. For example, RF devices complying

with WiGig are increasing in number. The availability of WiGig routers, such as the TP-Link Talon AD7200 [23] and the Netgear Nighthawk R9000-100EUS [24], and WiGig laptops such as the Dell Latitude [25], bring to practice multi-Gbps implementation of radio links for indoor scenarios. However, the offer of RF Commercial Off-The-Shelf (COTS) products for research purposes at mmWave band is yet to be satisfactory. To authors' knowledge, there are only two (cutting-edge) RF front-ends at 60 GHz available, namely EK1HMC6350 [26] and VUBIQ PEM009 [27], supplied by Analogue Devices (AD), and Pasternack, respectively. In both development systems, analogue upconversion/downconversion stages are implemented in a single TX/RX chip-set, with the claimed specifications presented in Table 1. From this table, it can be seen that both mmWave RF front-ends have similar features. However, differences arise in terms of noise figure value, where EK1HMC6350 has 2 dB more than PEM009, and surprisingly, supporting higher modulation orders.

TABLE 1. RF Front-ends features at 60 GHz.

Feature	Value	
Model	EK1HMC6350	PEM009
Technology	BiCMOS	CMOS
Frequency Range [GHz]	57 to 64	57 to 64.8
I/Q Interface	✓	✓
Suggested Modulation	Up to 64-QAM	4/16-QAM
Modulation Bandwidth [GHz]	1.8	1.8
RX Noise Figure	8 dB	6 dB

In the scope of enabling 5G communications, this paper presents an extensive study on the feasibility of COTS PEM009 RF front-end at mmWave band, comparing it against a reference RF front-end system. Therefore, detailed measurement analysis on the impact that RF impairments, induced by both systems under test, on the performance degradation of a Orthogonal Frequency Division Multiplexing (OFDM) system, based on the LTE standard, is considered. For this assessment, key performance indicators for QoS in digital communications such as Error Vector Magnitude (EVM), and Bit Error Rate (BER) were considered. The baseband of the OFDM transceiver is based on the authors work presented in [28]. In fact, the same fully pipelined hardware architecture is used to implement an over-the-air OFDM transceiver. However, in this work, the baseband bandwidth has been increased from 61.44 to 156.25 MHz and implemented in a Xilinx Virtex7 XC7VX485T Field Programmable Gate Array (FPGA), resulting in 1 Gbps of real-time transmission rate. In addition, PN, mixer IQ imbalances and PA non-linearities characterization for the PEM009 VUBIQ RF system is assessed. Furthermore, for performance comparison purposes, a research RF front-end (using only discrete connectorized analogue components) is used as reference.

R. Gomes *et al.*: Will COTS RF Front-Ends Really Cope With 5G Requirements at mmWave?

IEEE *Access*

With this, it is possible to verify which one is more suitable to tackle the 5G demands, or in other words, whether the current Integrated Circuit (IC) technology on RF circuits is ready for 5G deployment systems.

Despite the fact that in the datasheet of EK1HMC6350 system, 64-QAM capability is claimed, the work reported in [29], shows that signal modulation using such front-end is limited to 4-QAM (EVM at RX higher than 24%). Moreover, a literature survey reveals a lack of documentation addressing the usage of EK1HMC6350 system is presented in the literature. In fact, to the author's knowledge, only [29] was found. On the other hand, several scientific articles might be found on the VUBIQ system. For example, in [30]–[32] such system is employed for high precision tracking of people and objects while in [33] and [34] it is used for beamforming and beamstering. Finally, in [35] it is used to assess received signal power in beamforming and interference measurement setups. Based on such wide availability of information, the PEM009 is considered in this work.

The paper is organized as follows. Section III, introduces the Software Defined Radio (SDR) considered for wireless communications prototyping, and its magnitude frequency response characterization. In addition, the OFDM system design parameters and its performance in a Back-to-Back (B2B) scenario is presented. Section IV, details the RF architecture of PEM009. Section V, provides the RF non-linearities characterization for PEM009, measurement results in terms of TX/RX Intermodulation Distortion (IMD) products, TX/RX gain, TX carrier and signal leakages, RX clock leakages and power sensitivity. Also, the overall PEM009 magnitude response, IQ imbalances and Carrier Frequency Offset (CFO) are measured. In section VI, results of the OFDM performance at 60 GHz using PEM009 are shown. In section VII, the reference RF front-end architecture is presented, as well as, its corresponding performance results. In addition, a practical EVM link budget formulation is proposed in section VIII. Finally, main conclusions are drawn in section IX.

II. STATE OF THE ART ON MMWAVE TESTBED SYSTEM SPECIFICATIONS

5G is envisaged to deliver hundreds MHz of continuous spectrum and multi-Gbps transmission rates to mobile devices. To fulfill such requirement, mmWave frequency spectrum will be the enabling key technology [36]. The bandwidth available at the 60 GHz unlicensed band [37] may accommodate the entire radio communications operating from nearly DC up to 9 GHz. Another remarkable feature arises from the $1 - 2$ dB excess loss per km, at certain mmWave frequencies, in relation to that usually obtained directly from Friis' equation [36]. Due to this fact, mmWave communication systems are currently subject of a great deal of interest within the wireless scientific community. The 5G network minimum technical performance specifications have already been established [38]. For example, the peak data-rate and spectral efficiency in Downlink (DL) is 20 Gbps and

30 bps/Hz, respectively. For Uplink (UL) connection, values are half the DL ones. User data-rate and average spectral efficiency should be 100 Mbps (DL) and 50 Mbps (UL), and 7.8 bit/s/Hz (DL) and 5.4 bit/s/Hz, respectively, in a dense urban environment. System bandwidth should be at least 100 MHz, and the spectrum ranging from 24 to 100 GHz. Considering this, the authors' have presented in Table 2 a list of the most relevant mmWave testbeds available in the literature, along with their system specifications. Each testbed/prototype is summarized in terms of its affiliation, frequency band, base-band real-time signal processing, transmission scheme, system bandwidth, whether the transmission is over-the-air or not, and both system's maximum spectral efficiency per stream (not considering MU-MIMO) and Signal-Noise-to-Ratio (SNR). Whenever the SNR was not presented, this has been extrapolated from the minimum achieved EVM in the system performance.

Testbed systems listed in Table 2 demonstrate that it is possible to utilize the mmWave spectrum to successfully establish a radio link. However, only the testbeds reported in [39]–[42] consider a modulation bandwidth higher than 100 MHz, real-time baseband processing, and consider OFDM (the adopted waveform for the 5G New Radio (NR) [43]) as the transmission scheme. Moreover, it is evident that when using the 60 GHz band, there is a lack of testbeds which comply with the above specifications. Nevertheless, in all reported testbeds, spectral efficiency is rather low, i.e., the maximum QAM order is 64. Even in the listed 28 GHz testbed systems, such requirement should be further improved to meet the DL specification of 7.8 bit/s/Hz envisaged for 5G.

III. SOFTWARE DEFINED RADIO - OFDM TRANSCEIVER OVERVIEW

A SDR is a generic term for radio systems that employ the majority of Physical Layer (PHY) functionalities using Digital Signal Processing (DSP) algorithms, implemented in an embedded system with the aid of a specific software. For example, typical analogue stages such as mixing, amplification, filtering, modulation and demodulation, essential to establish a wireless radio link, are digitally implemented rather than using discrete hardware components. An ideal SDR is composed by an embedded platform engine and at least by one pair of Digital-to-Analogue Converter (DAC)/Analogue-to-Digital Converter (ADC) to translate signals from digital domain to analogue domain, and vice-versa. To this extent, in this work, the VC707 FPGA board is considered as the processor engine, which is one of the most powerful (with more logic resources) Xilinx FPGA's available on the market. The selection of both DAC and ADC was based on the criteria of sampling rate, binary resolution and compatibility with VC707 FPGA development board. According to Xilinx documentation [51], FMC 230 (DAC) and FMC 126 (ADC) from 4DSP, are the only converters meeting such requirements, available in the market. Furthermore, both DAC and ADC are configured for a sampling

IEEEAccess·

R. Gomes *et al.*: Will COTS RF Front-Ends Really Cope With 5G Requirements at mmWave?

TABLE 2. Current mmWave testbeds.

Ref.	Affiliation	Freq. Band [GHz]	Transmission scheme	BW [GHz]	real-time	over the air	MAx. Spectral eff. [bit/s/Hz]	Max. SNR [dB]
					Main Features			
[44]	Tokyo Institute of Technology	**60**	OFDM	2.16	no*	no	6	25.8
[45]	OpenMili	**60**	OFDM	0.0005	yes	yes	1	30
[46]	UESTC	**60**	SC	2.16	yes	yes	2	16.5
[39]	Samsung/ NTT DOCOMO	28	OFDM	0.8	yes	yes	4	$21^{\dagger}$ / $<28^{\dagger\dagger}$
[40]	NTT DOCOMO	28	OFDM	0.8	N/A	yes	6	N/A
[41]	ONRGET	28	OFDM	0.125	yes	yes	6	28
[42]	mmMAGIC	28	OFDM	0.12288	yes	yes	4	28
[42]	mmMAGIC	82	OFDM	0.12288	yes	yes	4	24
[47]	MiWaveS	**60**	SC	0.75	yes	yes	4	16.5
[48]	HUB/UFAF	**60**	OFDM	0.625	no*	yes	1	N/A
[29]	KTH / BLUEWAVE	**60**	OFDM	0.022	no*	yes	2	13.5
[49]	USW	**60**	SC	0.035	yes	yes	4	28.5
[50]	Nokia /NTT DOCOMO	73.5	SC	1	yes	yes	4	18
N/A	**our USW/IT tesbed**	**60**	**OFDM**	**0.156**	**yes**	**yes**	**8**	**37.81**

(*) OFDM TX/RX processing is performed off-line by an host PC.
($\dagger$) Outdoor environment.
($\dagger\dagger$) Indoor environment.

frequency of 1.25 GHz. Low pass filters are considered to filter, at the DAC output, Nyquist replicas of the transmitted signal.

Following the specification presented in [38] for 5G pre-trials (BW higher than 100 MHz), a multi-Gigabit real-time OFDM TRX engine (testbed), implemented in a VC707, was developed based on the LTE standard, targeting the downlink PHY layer [2], with the operating parameters given in Table 3, for both 4-, 16-, 64-, and 256-QAM. Nevertheless, all algorithms needed for an over-the-air transmission, namely, timing and frame synchronization, channel estimation and equalization, and CFO compensation are considered, following the work presented in [28]. In addition, to anticipate OFDM performance degradation due to

IQ imbalances from the RF front-end, a digital IQ mixing stage, also known as Digital Up-Converter (DUC), was also implemented, and thus signals are transmitted from the SDR in low Intermediate Frequency (IF) modulation. Considering this, OFDM might be transmitted centered at four IF possibilities, such as: zero IF (DC), IF2 (156.25 MHz), IF4 (312.5 MHz), and IF6 (468.75 MHz). At the receiver, following a Digital Down-Converter (DDC), both decoded bitstream data or equalized QAM constellation symbols are acquired with the aid of a real-time debugging tool. A Xilinx Integrated Logic Analyzer (ILA) is utilized to perform several sample acquisitions and transmit them to a host PC for post-processing, enabling BER and EVM calculations. In sum, SDR system specifications are presented in Table 4.

R. Gomes et al.: Will COTS RF Front-Ends Really Cope With 5G Requirements at mmWave?

IEEE Access

TABLE 3. Main parameters considered in the design of OFDM system, based on the LTE [2] standard.

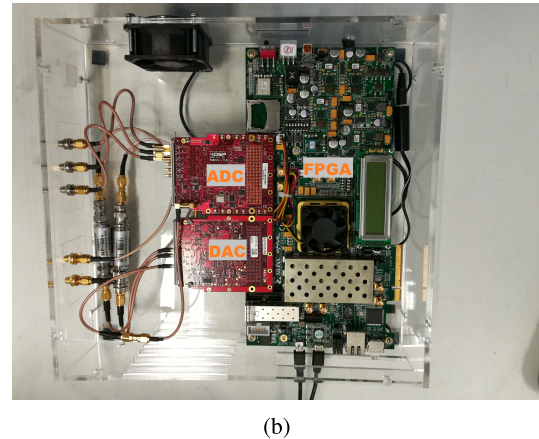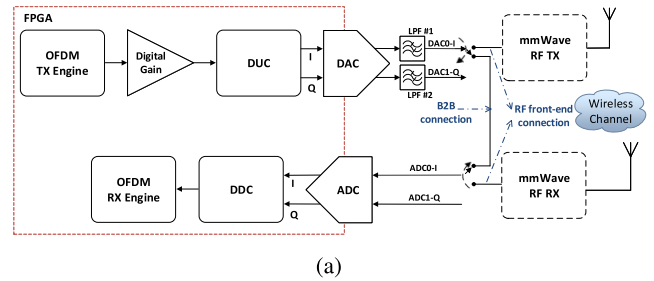| Parameter	Value
FFT size block	1024
Data block size	800
Sub-carrier bandwidth	152 kHz
Modulation	16/64/256-QAM
Guard time interval	256 samples
Maximum data-rate	1 Gbps

TABLE 4. Considered SDR system specifications.

Feature	Value
Processing BW	1.25 GHz
Transmission BW	150 MHz
ADC/DAC sampling rate	1.25 Gsamples/s
Modulation	OFDM 4/16/64/256-QAM
Max spectral eff.	8 bits/s/Hz/user
IF freq.	DC-612 MHz
User configuration	Single
Antenna configuration	SISO
Number of DAC/ADC channels	2/3
Resolution of DAC/ADC	14/10 bits

(a)

(b)

FIGURE 1. Considered SDR: block diagram a) and picture b) of the developed system for wideband signals.

From this table, it is evident that the proposed baseband OFDM testbed meets the 5G peak spectral efficiency value of 7.8 bit/s/Hz [38]. Additionally, when the proposed SDR is connected to a mmWave RF front-end, the gap verified in section II for testbeds operating at 60 GHz may be fulfilled. In other words, no other prototype system can process a signal BW of 150 MHz in real-time, with modulation orders up to 256 QAM, using OFDM as transmission scheme in over-the-air scenario. Both block diagram and picture of the developed TRX are depicted in Fig.1a, and 1b, respectively.

A. SDR MAGNITUDE FREQUENCY RESPONSE
In an over the air transmission, not only the RF front-end is responsible for distorting baseband signals. In fact, both DAC and ADC might induce non-linearities, which also affect both transmitter and receiver performances. For example, considering the Frequency Response (FR) of FMC230 channel 0, shown in Fig. 2a, it is clearly seen that Voltage Peak-to-Peak (Vpp) is not constant for different frequency tones. From Fig. 2b, it is also verified a poor DAC performance around DC, exhibiting maximum of 46 dB of signal attenuation at 50 kHz, and 10 dB from 224 MHz up to 312 MHz. The same analysis has been conducted for the FMC126 daughter board, and is presented in Fig. 3.

For the Wideband (WB) OFDM TRX introduced in section III, the DAC/ADC FRs are particularly relevant. A Time-Domain (TD) Constant Amplitude Zero Autocorrelation (CAZAC) Zadoff-Chu sequence is used for synchronization and CFO estimation. This sequence is composed by a set of subcarriers around DC, and therefore significant

attenuation will be experienced, which might lead to a significant performance degradation in estimation of both the beginning of OFDM frame samples and CFO value.

B. BASEBAND OFDM SYSTEM PERFORMANCE
The performance of the OFDM TRX, in a B2B configuration, is evaluated using EVM as QoS assessment metric. Moreover, the OFDM signal output power can be changed according to a gain selection on a digitally controlled amplification stage. Figure 4, shows the output power transfer curve as a function of selected gain and IF modulations. It is verified that OFDM modulation centered in IF2 provides higher DAC output power than the remaining IF frequencies, since less signal attenuation occurs at this frequency, in comparison with the other IF values.

TABLE 5. Summary of the system OFDM performance, in B2B configuration, for various IF values, DAC/ADC channel configurations, and max. digital gain.

IF config.	EVM I [%]	EVM I [dB]	EVM Q [%]	EVM Q [dB]	EVM IQ [%]	EVM IQ [dB]
0	-	-	-	-	320.76	11.17
2	0.85	-41.29	**0.77**	**-42.21**	4.36*	-27.16*
4	**0.84**	**-41.51**	0.78	-42.10	0.87	-41.23
6	0.97	-41.22	0.90	-40.86	**0.72**	**-42.75**

(*) Received level power exceeds the ADC saturation point.

From Table 5, EVM results are summarized for a digital gain of 7 (maximum gain), and for four different low
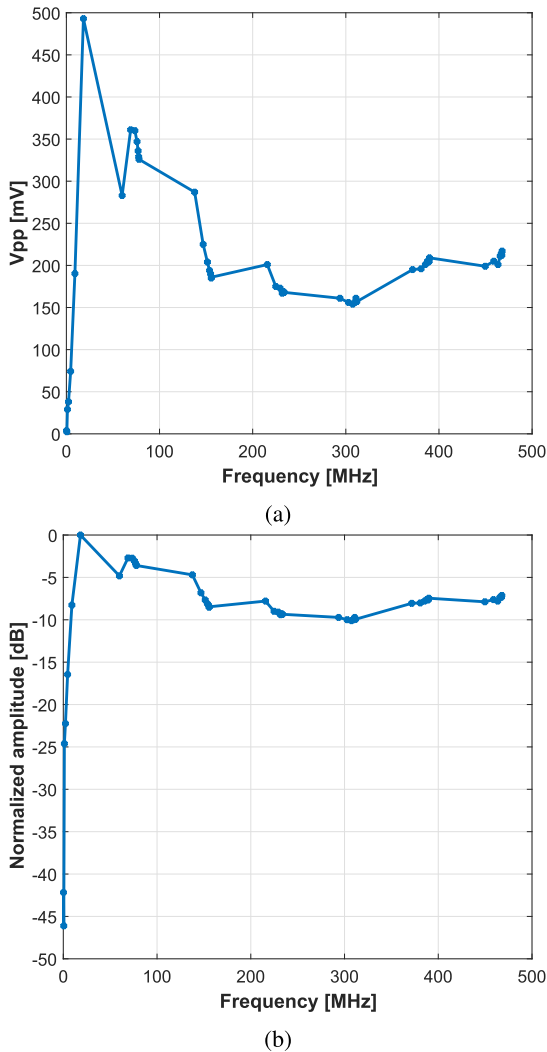
IEEE *Access*

R. Gomes *et al.*: Will COTS RF Front-Ends Really Cope With 5G Requirements at mmWave?

FIGURE 2. DAC magnitude frequency response representation for the DAC0 channel in: a) Vpp, and b) normalized amplitude.

FIGURE 3. ADC magnitude frequency response representation for the ADC0 channel in: a) Vpp, and b) normalized amplitude.

IF configurations. Additionally, when either I or Q channels are used to transmit and receive data, EVM results are denoted *EVM I* or *EVM Q*, respectively. This is, connecting DAC0 to ADC0 is considered as the *I branch*, and connecting DAC1 to ADC1 channels is the *Q branch*, as illustrated in Fig. 1a. Additionally, for a quadrature transmission, both I/Q channel branches are used simultaneously. These results show that a minimum EVM of approximately -42 dB is obtained for all low IF modulations, except for zero-IF (synchronization algorithms fails to estimate the beginning of frame), due to the nulls obtained on both DAC/ADC FRs. As expected, for other IFs, no OFDM performance degradation is verified, even when an IQ transmission configuration is considered, indicating that very low distortion is present on received signal constellations. As it can be seen in Fig.5, considering IF2 frequency and a maximum digital gain, 4- and 256-QAM constellations do not present significant scattering distortion on the received symbols. This subjective quality evaluation indicates that the OFDM SDR system is very accurate.
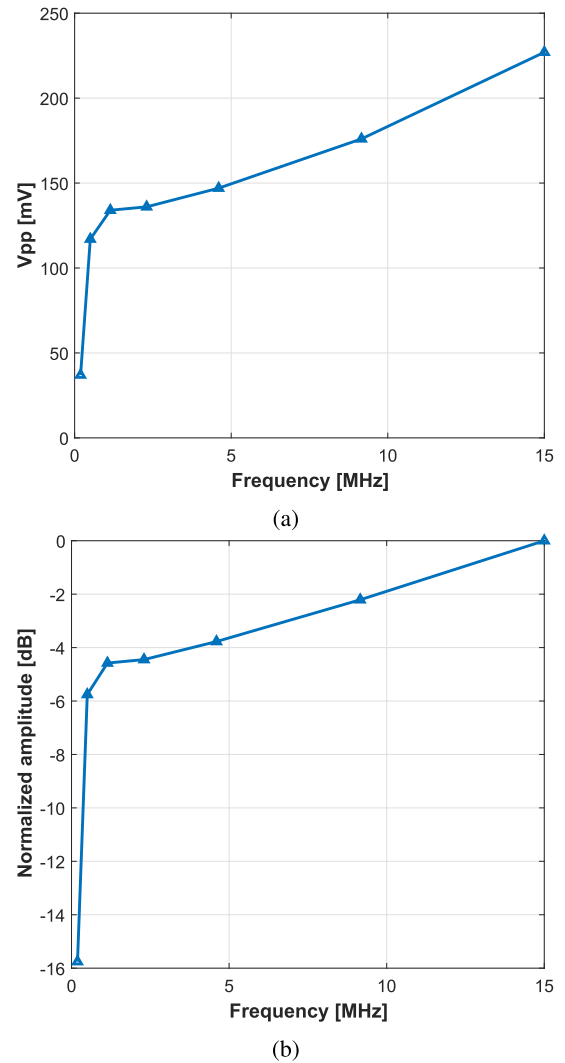
IV. PEM009 ARCHITECTURE OVERVIEW
The VUBIQ PEM009 RF Front-End, is a TX/RX 60 GHz development system, which can be configured by a host PC via USB interface [27]. A Graphic User Interface (GUI) allows to change multiple parameters such as: signal attenuation, baseband filter bandwidth, channel spacing and center frequency. Both boards (TX and RX) have built-in reference clocks at 308.571 MHz. However, in order to ensure that the clock signal can be used in a shared TX/RX configuration (avoiding CFO between TX/RX boards), a Clock (CLK) generator board using an external clock crystal was developed with the same frequency of the built-in clock. This reference clock enables center frequency (f_C) steps from 57.24 to 64.8 GHz. In the following subsections, details regarding TX/RX boards and the developed clock board are given.

A. TX BOARD
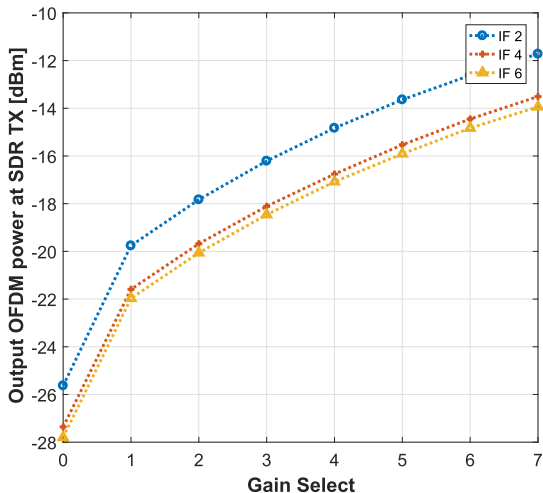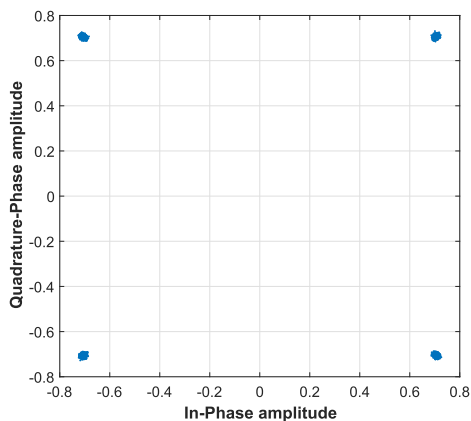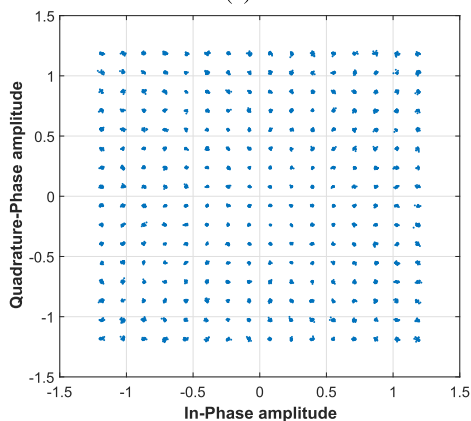At the VUBIQ TX board, both IQ differential baseband signals are upconverted into a 60 GHz RF signal through

R. Gomes *et al.*: Will COTS RF Front-Ends Really Cope With 5G Requirements at mmWave?

IEEE *Access*

FIGURE 4. OFDM transmitted signal power versus digital gain, and IF frequency.

(a)

(b)

FIGURE 5. B2B scatter constellation plots for: a) 4-QAM and b) 256-QAM, considering *IF* 2 and max. digital gain.

a two mixer stage, as it can be seen in Fig. 6. First an IF IQ mixer, operating at a Local Oscillator (LO) frequency (f_{LO1}), translates and combines both IQ baseband signals,
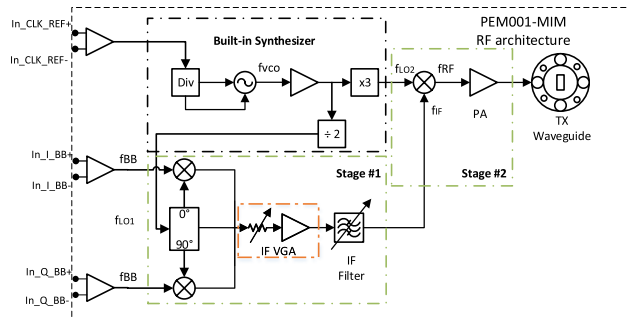

FIGURE 6. PEM009 transmitter two-step superheterodyne architecture (adapted from [27]).

at Baseband Frequency (f_{BB}), into a single signal centered at an intermediate frequency (f_{IF}). Next, an amplification stage is presented followed by a bandpass filter to suppress unwanted image signals. The gain in this IF branch might also be reduced through an IF attenuator (IF_{Att}). Finally, this intermediate signal is modulated to a central carrier frequency, f_C, through a second mixing stage (operating at f_{LO2}). Both f_{LO1}, f_{LO2} and Voltage-Controlled Oscillator (VCO) frequencies (f_{VCO}) are generated in the built-in synthesizer, which requires a external differential reference clock signal (In_CLK_REF$^+$/In_CLK_REF$^-$), to lock its Phase Lock Loop (PLL). The relation between all these signal frequencies is given by the following equations:

$$\begin{cases} f_{LO1} = fvco \times \frac{1}{2} \\ f_{LO2} = 3 \times fvco \\ fvco = f_C \times \frac{2}{7} \\ f_{RF} = f_C + f_{BB} \\ f_{IF} = f_{LO1} + f_{BB} \end{cases} \quad (1)$$

where f_{RF} is the transmitted signal frequency.

B. RX BOARD
At RX, the counterpart of the TX upconversion process is performed, in two stages. Firstly, the received mmWave signal is amplified by a Low-Noise Amplifier (LNA). Secondly, a frequency down-conversion is made with the first LO moving the RF signal down to the IF band. This is followed by amplification and filtering stages, which suppress image signals and adjusts signal levels for optimum I/Q demodulation. Next, downconversion to baseband with an I/Q mixer is carried out. Finally, additional gain-control and anti-aliasing filtering might be performed in the demodulated baseband signal, as illustrated in Fig. 7.

C. DEVELOPED EXTERNAL CLK BOARD
The reference clock source of both TX and RX devices might be shared to avoid additional distortions effects due to CFO. However, in a realistic environment scenario, both TX and RX are operating using independent clock sources, and thus CFO is inherently present. The bounds of the
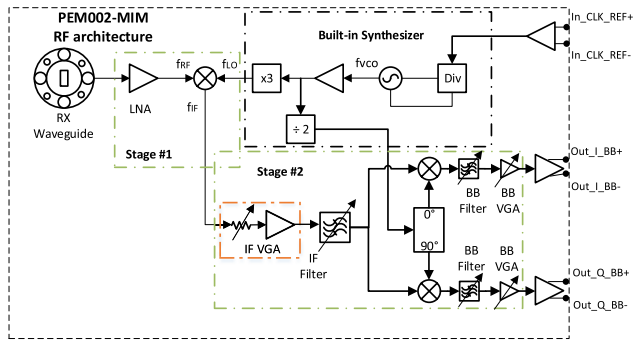
IEEE *Access*

R. Gomes *et al.*: Will COTS RF Front-Ends Really Cope With 5G Requirements at mmWave?

FIGURE 7. PEM009 two-step superheterodyne downconversion architecture presented in the receiver (adapted from [27]).

TABLE 6. Measured phase noise of M6300 oscillator clock, at 308.571 MHz.

Freq. Offset [Hz]	Phase Noise [dBc/Hz]
10	-62
100	-78.5
1000	-80
10000	-99
100000	-118
1000000	-124

frequency difference between TX and RX clocks, can be computed from the frequency stability of the crystal oscillators located in each of TX/RX boards. For example, the ±25 ppm crystal oscillator implemented in both TX/RX boards of the PEM009, induces a maximum frequency shift between TX/RX of 1.5 MHz (considering a 60 GHz RF carrier). This impairment value may be impractical for some wireless PHY layers, and thus, a new crystal-based clock has been developed and attached at both TX/RX equipments, as shown in Fig. 8. The chosen crystal oscillator was the M6300 supplied by MtronPTI, and has the following features: LVPECL differential output at 308.571 MHz, and frequency stability of ≈ 0.5 ppm. The M6300 clock measured phase-noise values at 100 Hz, 1kHz and 10 kHz are given in 6.
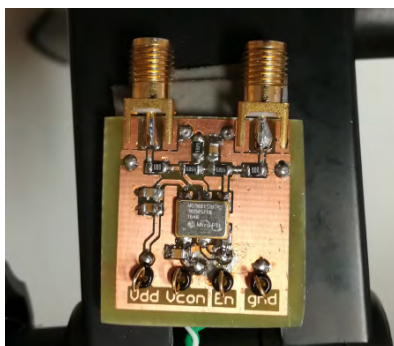

FIGURE 8. Developed external reference clock source (M6300 oscillator) board.

Consequently, using such oscillator, the CFO presented in the PEM009 is now reduced to a maximum theoretical value of 30 kHz.

V. PEM009 RF IMPAIRMENTS CHARACTERIZATION

In this section the RF impairments of the PEM009 VUBIQ 60 GHz development system [27] are assessed. Its TX board is therefore, characterized in terms of transmitted power, carrier and side-band RF leakages and IMD products. Similar measurements were conducted on the RX board. In addition, the system is characterized by its IF-IF frequency response magnitude, IQ and DC voltage offset imbalances. These results will be essential for mmWave RF impairments modelling, for the design of appropriate digital signal processing compensation algorithms, and, ultimately, for EVM link budget estimation purposes.
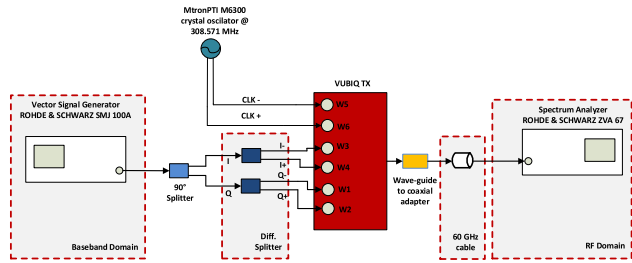
A. TRANSMITTER

1) OUTPUT POWER AND GAIN

Although several amplification stages are present and embedded in the mmWave TX, as seen in Fig. 6, no information regarding their gains are provided [52]. Therefore an extensive RF measurement on the TX output power was conducted. The utilized setup for such experiment is illustrated in Fig. 9, where the TX board input Continuous Wave (CW) signals are generated by a Vector Signal Generator (VSG) (ROHDE & SCHWARZ SMJ 100 A), an then split into two similar branches. Since TX input connector ports are differential, a 180° splitter is used to convert both single-ended interfaces into differential ones. The signal power level of both baseband signals is set to the recommended −26 dBm value. Finally, the output signal power is measured by connecting the mmWave TX wave-guide port to the ZVA 67 Vector Network Analyzer (VNA), operating in Spectrum Analyzer (SA) mode. Results are summarized in Fig. 10, considering single tone baseband signals of 10 MHz (f_{FO}), and f_C values of 57.24 GHz, 59.4 GHz, 61.56 and 63.72 GHz. Average output power levels of 4, −4 and −23 dBm were obtained for IF_{Att} values of 0, 8 and 20 dB, respectively. Moreover, Fig. 11a shows the output signal power dependency on IF_{Att} values at $f_{RF} = 57.25$ GHz. It can be clearly seen that the analogue IF attenuator does not changes linearly with the GUI configuration value. A maximum gain of 32 dB, was obtained for an IF_{Att} of 0 dB, as it is illustrated in Fig. 11b.

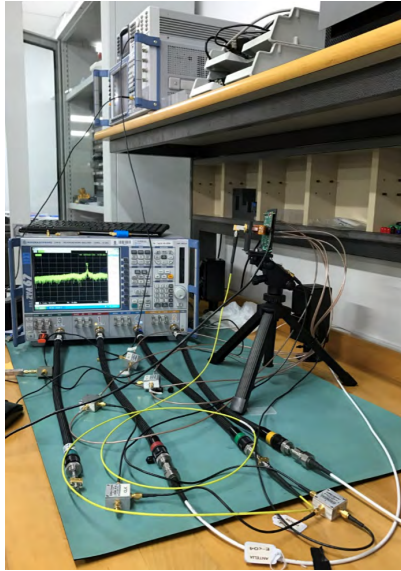#### 2) INTERMODULATION DISTORTION PRODUCTS

Non-linear distortion in wireless RF Front-Ends are usually characterized by 2nd and 3rd-order IMD products. Such products are mainly generated by cascaded amplifiers and mixers present in the upconversion, due its analogue design architecture. Power levels of both 2nd and 3rd distortion products are measured at the output of TX board, utilizing the same measurement setup of Fig. 9. However, a baseband signal consisting of two tone frequencies, at 50 MHz and 52.44 MHz, is considered instead.

The power level difference between 2nd and 3rd intermodulation products and both fundamental tones are presented (in dBc values) in Tables 7, 8, 9 and 10, for f_C values of 57.24,

R. Gomes *et al.*: Will COTS RF Front-Ends Really Cope With 5G Requirements at mmWave?

IEEE *Access*

(a)

(b)

FIGURE 9. Block diagram of the transmitted output power measurement setup in a), and its picture in b).
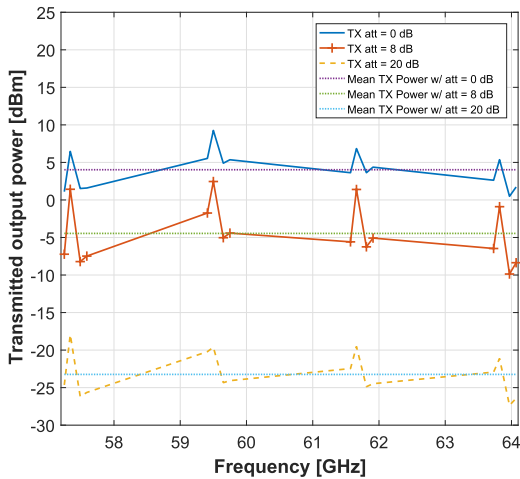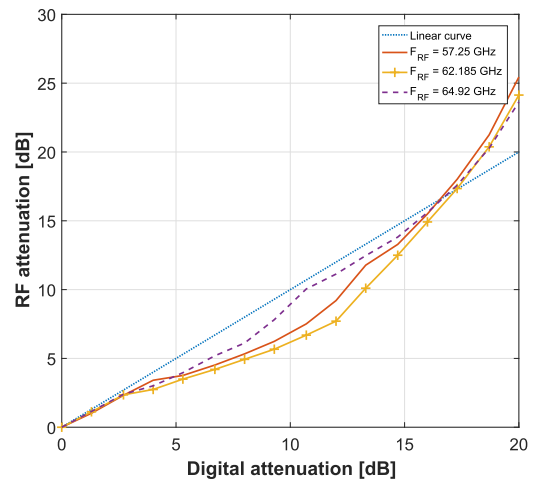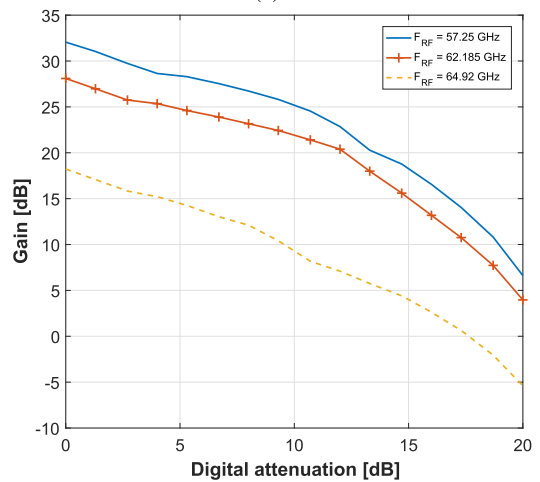

FIGURE 10. Transmission output power performance versus f_{RF} and IF_{Att} values.

59.4, 61.56 and 63.72 GHz, respectively. Additionally, for each of the f_C values, 0, 8, 12 and 20 dB values for IF_{Att} are used.

Moreover, the most significant IMD products (lowest IMD dBc value) are shown in Fig.12, for each f_C and IF_{Att} combinations. As it is depicted, and as expected, the power ratio

(a)

(b)

FIGURE 11. Digital attenuation values versus: a) RF attenuation, and b) signal gain, considering a input power of −26 dBm.

TABLE 7. Power level difference between IMD products and both fundamental tones, considering f_C = 57.24 GHz.

IMD product	Relative Power [dBc]			
	Att. = 0*	Att. = 8*	Att. = 12*	Att. = 20*
f_2-f_1	35.37	38.32	38.84	39.44
$2f_1$-f_2	30.4	29.06	**26.51**	39.56
f_1	-0.8	-0.52	-0.47	-0.7
f_2	0	0	0	0
$2f_2$-f_1	**28.36**	31.22	31.33	39.56
$2f_1$	42.32	43.54	45.07	38.95
f_1+f_2	36.96	37.52	37.83	38.92
$2f_2$	43.86	43.82	45.71	**38.88**
$3f_1$	37.11	37.42	39.17	39.12
$2f_1$+f_2	28.45	**27.56**	27.8	39.14
f_1+$2f_2$	29.18	28.04	28	39.18
$3f_2$	39.38	38.74	40.61	39.21

(*) in dB.

between IMD products and carrier increases as the digital attenuation increases. This implies that cascaded amplifiers start operating far below their saturation point as the IF

IEEE *Access*

R. Gomes *et al.*: Will COTS RF Front-Ends Really Cope With 5G Requirements at mmWave?

TABLE 8. Power level difference between IMD products and both fundamental tones, considering f_C = 59.4 GHz.

IMD product	Relative Power [dBc]			
	Att. = 0*	Att. = 8*	Att. = 12*	Att. = 20*
f_2-f_1	32.36	42.75	35.8	40.03
$2f_1$-f_2	37.53	**30.24**	**27.42**	40.42
f_1	-1.63	-0.97	-1.29	-1.27
f_2	0	0	0	0
$2f_2$-f_1	**23.58**	34.12	30.11	40.67
$2f_1$	38.29	46.97	43.99	42.09
f_1+f_2	33.63	41.78	37.5	42.12
$2f_2$	41.05	48.29	44.05	42.16
$3f_1$	32.05	41.33	37.95	41.39
$2f_1$+f_2	23.59	32.67	28.18	**39.35**
f_1+$2f_2$	24.44	33.45	28.28	41.23
$3f_2$	35.4	43.11	39.14	41.18

(*) in dB.

TABLE 9. Power level difference between IMD products and both fundamental tones, considering f_C = 61.56 GHz.

| IMD product	Relative Power [dBc]			
	Att. = 0*	Att. = 8*	Att. = 12*	Att. = 20*
f_2-f_1	31.79	43.13	35.27	39.18
$2f_1$-f_2	33.11	33.28	**26.38**	37.84
f_1	-1.63	0	0	-1.99
f_2	0	-1.41	-0.54	0
$2f_2$-f_1	**21.51**	32.41	29.5	39.40
$2f_1$	37.66	44.37	42.12	39.46
f_1+f_2	32.23	39	36.45	39.45
$2f_2$	40.82	47.08	42.63	39.44
$3f_1$	31.96	39.92	36.83	39.23
$2f_1$+f_2	23.91	30.98	28.43	**37.53**
f_1+$2f_2$	24.75	**31.22**	29.56	39.2
$3f_2$	37.42	41.75	37.69	39.18

(*) in dB.

TABLE 10. Power level difference between IMD products and both fundamental tones, considering f_C = 63.72 GHz.

IMD product	Relative Power [dBc]			
	Att. = 0*	Att. = 8*	Att. = 12*	Att. = 20*
f_2-f_1	37.28	42.38	36.63	36.3
$2f_1$-f_2	26.33	36.43	26.35	**35.33**
f_1	-3.65	-1.99	-0.64	-0.25
f_2	0	0	0	0
$2f_2$-f_1	26.17	32.61	32.44	37.62
$2f_1$	38.94	46.87	42.68	38.22
f_1+f_2	32.59	41.99	37.01	38.22
$2f_2$	40.17	48.33	43.62	38.21
$3f_1$	32.16	40.63	36.98	37.43
$2f_1$+f_2	**22.11**	28.42	25.72	37.36
f_1+$2f_2$	23.53	**27.57**	**25.58**	37.27
$3f_2$	36.43	37.88	37.56	37.21

(*) in dB.

attenuation is increased. The maximum difference between fundamental tones and IMD products power is 39.35 dBc, and happens for an IF$_{Att}$ equals to 20 dB and a f_C of 59.4 GHz.
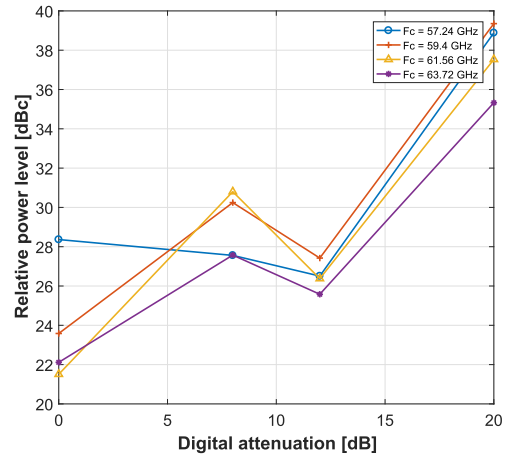
FIGURE 12. IMD product power when related to the carrier value, for each f_C and digital attenuation configurations.

Other figures of merit to evaluate IMD products are the 2nd and 3rd order Intercept Points, IP2 and IP3, respectively. Such values indicate when both 2nd/3rd order power levels overtake the fundamental tone, at a particular input power. IP2 and IP3 are constituted by two coordinate points, Input Intercept Point (IIP_n) and Output Intercept Point (OIP_n), where n indicates the IMD order. The OIP_n is defined as follows:

$$OIP_n = P_{out} + \frac{\Delta P}{n-1}, \qquad (2)$$

where, P_{out} and ΔP denote the fundamental tone output power and the difference between P_{out} and the IMD product power level, respectively. Consequently, IIP_n can be obtained by:

$$IIP_n = OIP_n - G, \qquad (3)$$

where, G is the linear gain of the device.

Particularly, for the VUBIQ TX (input power is constant), only OIP_2 and OIP_3 values are measured. Furthermore, OIP_2 is obtained considering the IMD tone of $f_1 + f_2$, and OIP_3 is calculated by:

$$\begin{cases} OIP_{3(low)} = P(f_1) + \dfrac{P(f_2) - P(2f_1 - f_2)}{2} \\[2mm] OIP_{3(high)} = P(f_2) + \dfrac{P(f_1) - P(2f_2 - f_1)}{2}, \end{cases} \qquad (4)$$

where, $P(2f_1 - f_2)$ and $P(2f_2 - f_1)$ are the power of the low and high frequency signals of the intermodulation signal, respectively.

The obtained values for OIP_2 is given in Table 11 considering the same TX parameter combinations of previous measurements. Similarly, values for OIP_3 are shown in Table 12 for a f_C of 57.24 GHz and 59.4 GHz and in Table 13 OIP_3 for 61.56 GHz and 63.72 GHz.

R. Gomes et al.: Will COTS RF Front-Ends Really Cope With 5G Requirements at mmWave?

IEEE *Access*

TABLE 11. Measured OIP_2 values considering a f_C of 57.24 GHz, 59.4 GHz, 61.56 GHz and 63.72 GHz.

Att. [dB]	OIP$_2$ [dBm]			
	57.24 GHz	59.4 GHz	61.56 GHz	63.72 GHz
0	42.32	41.76	38.21	33.72
8	36.37	45.25	40.55	40.83
12	31.99	36.6	32.96	30.48
20	15.98	15.98	17.19	15.53

TABLE 12. Measured $OIP_{3(low)}$ and $OIP_{3(high)}$ values for f_C = 57.24 GHz and f_C = 59.4 GHz.

|	F$_c$ = 57.24 GHz		F$_c$ = 59.4 GHz	
Att. [dB]	OIP$_{3(low)}$ [dBm]	OIP$_{3(high)}$ [dBm]	OIP$_{3(low)}$ [dBm]	OIP$_{3(high)}$ [dBm]
0	21.36	19.94	28.52	20.74
8	13.9	14.72	19.56	21.01
12	7.89	10.06	14.1	14.8
20	-2.46	-2.81	1.62	1.11

TABLE 13. Measured $OIP_{3(low)}$ and $OIP_{3(high)}$ values for f_C = 61.56 GHz and f_C = 63.72 GHz.

|	F$_c$ = 61.56 GHz		F$_c$ = 63.72 GHz	
Att. [dB]	OIP$_{3(low)}$ [dBm]	OIP$_{3(high)}$ [dBm]	OIP$_{3(low)}$ [dBm]	OIP$_{3(high)}$ [dBm]
0	24.16	17.55	17.96	16.05
8	17.48	17.75	19.04	16.14
12	9.42	11.25	6.96	10.01
20	-1.35	-1.57	-4.77	-3.75

3) RF CARRIER AND SIDE-BAND LEAKAGES

Usually in IQ upconversion architectures, such as the one represented in Fig. 6, not only the modulated signal is transmitted, but also its undesired image and RF carrier, which may harm adjacent wireless channels. The transmission of an undesired RF carrier results from the presence of DC voltage offset in both I/Q branches that can be either introduced by both I and Q signal inputs or from analogue hardware imperfections present in the RF modulator.

In order to evaluate both undesired signals at the PEM009 TX board, metrics as carrier and image (also known as side-band) leakages, are considered. Both metrics measure the power level difference between both desired and undesired transmitted signals. For this system analysis, the measurement setup of Fig. 9 is considered, as well as, using the same input TX combination parameters of previous analysis. The summary of these results are detailed in Fig. 13. As it can be seen from this figure, although a carrier suppression is verified in average, around 11 dBc, for IF_{Att} = 20 dB, the side-band leakage presents more power than the desired signal (also in average). For example, a −1.6 dBc value is verified for IF_{Att} = 0 dB. Therefore, according to these results, TX board induces relevant IQ imbalances into baseband signals.
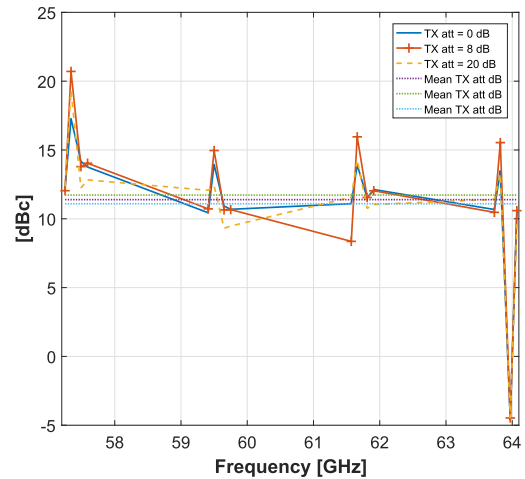
(a)
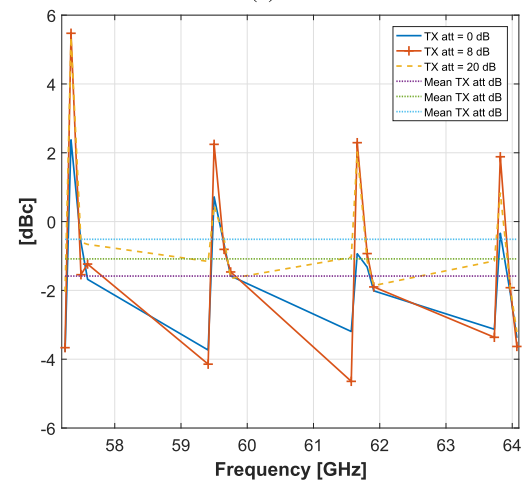
(b)

FIGURE 13. Both carrier a) and b) side-band suppressions, considering different combinations of f_C and f_{FO} frequency values.

B. RECEIVER

In this subsection, a detailed RF characterization analysis is performed on the mmWave integrated PEM009 receiver chipset. Clock and synthesizer leakages, IMD products and power sensitivity are the considered metrics for such evaluation.

1) DIRECT CLOCK LEAKAGES

In order to investigate and identify possible hardware imperfections on the receiver side, a spectrum analysis on the received baseband signal is performed when the RX board is either turned OFF or ON. In this way, one can not only verify possible direct leakages from the clock source, but can also evaluate possible synthesizer leakages into both baseband I/Q channels. The considered measurement setup is illustrated in Fig. 14.

From Fig. 15, results demonstrate that when RX is powered OFF, signal leakages from the external source clock are present in both I/Q channels, since its fundamental tone at 308.571 MHz and its third harmonic frequency component,
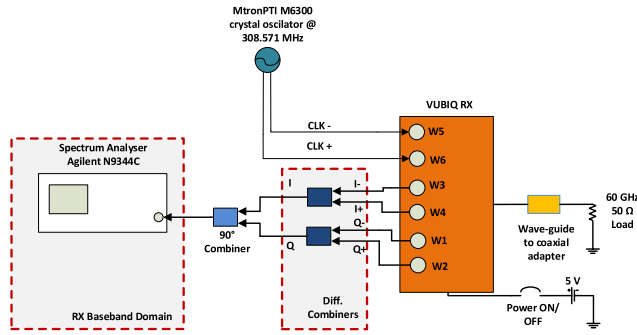
IEEE *Access*

R. Gomes *et al.*: Will COTS RF Front-Ends Really Cope With 5G Requirements at mmWave?

FIGURE 14. Block diagram of the clock leakage measurement setup.

FIGURE 16. Overlapped IQ baseband frequency responses for f_C values of 57.24 GHz, 59.4 GHz, 60.48 GHz, and for 63.72 GHz.

FIGURE 15. Direct signals leakage from the external clock reference signal to the baseband I/Q channels.

TABLE 14. Summary of 2nd and 3rd-order IMD products, considering f_C = 60.48 GHz, *RX IF*$_{\text{Att}}$ = 20 dB, and TX IF$_{\text{Att}}$ set from 0 dB up to 20 dB.

IMD product	Relative Power [dBc](*)			
	Att.$_{TX}$=0†	**Att.$_{TX}$=8**†	**Att.$_{TX}$=12**†	**Att.$_{TX}$=20**†
f_2-f_1	31.95	29.96	33.36	32.76
$2f_1$-f_2	**22.25**	22.3	**18.11**	**30.66**
f_1	-1.7	0	0	0
f_2	0	-0.4	-3.29	-1.04
$2f_2$-f_1	23.6	**21.5**	18.41	31.16
$2f_1$	40.26	38.2	39.11	‡
f_1+f_2	30.2	31.2	36.61	‡
$2f_2$	43.4	45.5	44.11	‡
$3f_1$	38	32.6	33.11	‡
$2f_1$+f_2	22.5	22.2	23.11	‡
f_1+$2f_2$	24.5	34.1	26.41	‡
$3f_2$	42	38.5	37.31	‡

(*) RX digital attenuation is fixed to 20 dB.
(†) in dB.
(‡) Not sufficient dynamic range available in the SA.

at 925.713 MHz, are approximately −78 dBm and −83 dBm, for I and Q baseband channels, respectively. As such, clock input ports are not isolated from I/Q RX baseband ports, exhibiting an attenuation of 68 dB (for a clock input power level of −10 dBm).

A similar study is carried out for all f_C values available in the RX input parameters (switching between 15 carriers spaced by 540 MHz), when RX is powered ON. These results are shown in Fig.16 for f_C values from 57.24 GHz up to 63.72 GHz. Moreover it is clearly seen that undesirable signal tones are present all over the system bandwidth, meaning that a WB received I/Q signal will be interfered with such leaks, unless f_C is chosen to be 60.48 GHz. At this frequency, the signal is able to lock without generating harmonics. In addition, from these results, it is demonstrated that the received signal noise floor of the RX is around −70 dBm, and −60 dBm, respectively for an IF digital attenuation of 0 dB and 16 dB. Therefore, leakages from the previous study (depicted Fig. 15) are masked by noise, not affecting the system performance.

2) INTERMODULATION DISTORTION PRODUCTS

The IMD products from 2nd and 3rd-order are now being evaluated on both received I/Q baseband channels, after
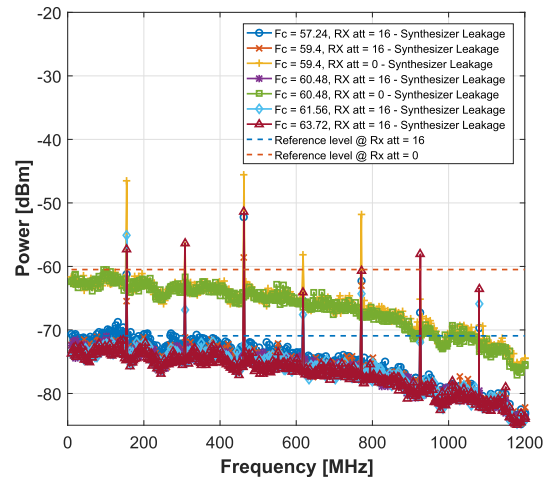
demodulation, instead of being measured at 60 GHz. The block diagram of the measurement setup is illustrated in Fig. 17. The signal is transmitted through a coaxial cable with enough attenuation to avoid the receiver saturation, and next, it is demodulated by the mmWave integrated RX IC and captured by an Agilent N9344C spectrum analyzer. Based on the receiver clock leakage results, a f_C equal to 60.48 GHz is chosen for this characterization.

The power level assessment for IMD products is performed also for different combination values of TX and RX IF$_{\text{Att}}$. While changing the TX IF$_{\text{Att}}$ from 0, 8, 12 and 20 dB, the RX IF$_{\text{Att}}$ values are fixed, and vice-versa.

From the above results, it is verified that in order to mitigate non-linearity effects from amplification stages, TX and RX IF attenuations must be set to 20 and 12 dB, respectively, for a power difference of 35 dBc between the fundamental tone and IMD products.
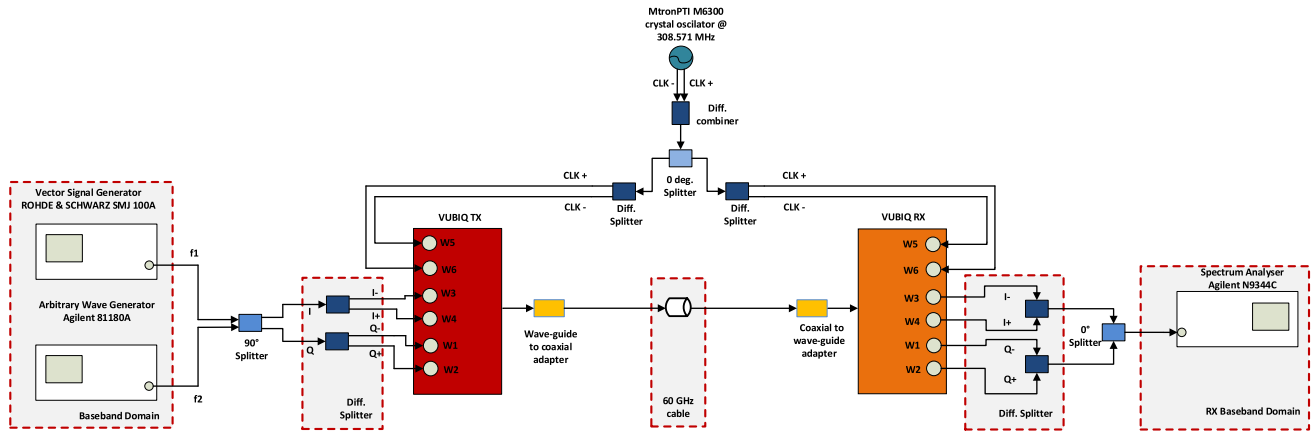
R. Gomes et al.: Will COTS RF Front-Ends Really Cope With 5G Requirements at mmWave?

IEEE Access

FIGURE 17. VUBIQ RX IMD characterization measurement setup.

TABLE 15. Summary of 2nd and 3rd-order IMD products, considering f_C = 60.48 GHz, $TX\ IF_{Att}$ = 20 dB, and RX IF_{Att} set from 0 dB up to 20 dB.

IMD product	Relative Power [dBc]$(^*)$		
	$Att._{RX}=0^{\dagger}$	$Att._{RX}=8^{\dagger}$	$Att._{RX}=12^{\dagger}$
f_2-f_1	61.6	56.8	53.4
$2f_1-f_2$	**33.3**	**34.6**	**35**
f_1	-1	-0.8	-0.5
f_2	0	0	0
$2f_2-f_1$	36.96	36.45	36.8
$2f_1$	‡	‡	‡
f_1+f_2	‡	‡	‡
$2f_2$	‡	‡	‡
$3f_1$	‡	‡	‡
$2f_1+f_2$	‡	‡	‡
f_1+2f_2	‡	‡	‡
$3f_2$	‡	‡	‡

$(^*)$ TX digital attenuation is fixed to 20 dB.
$(^{\dagger})$ in dB.
$(‡)$ Not sufficient dynamic range available in the SA.

3) RECEIVER POWER SENSITIVITY AND GAIN

To evaluate the receiver gain, it is necessary to assess the received power at the input port of the RX 60 GHz wave-guide. Therefore, taking into account the transmitted output power and the measurement setup illustrated in Fig. 17, the estimated received power level at the RX wave-guide can be calculated by:

$$P_r = P_t - L_{cable} - 2 \times L_{connector}, \quad (5)$$

where, P_r, P_t, L_{cable}, and $L_{connector}$, are the received power, transmitted power, cable, and connector losses, respectively. Hence, the received RF power for different combinations of f_C, and f_{FO} values, is given in Table 16.

Consequently, considering both received tones power levels at RF and baseband frequencies, it is possible to estimate the RX gain. For example, in Table 17, the RX overall gain is 49.2 and 44.2 dB for RX IF_{Att} values of 0 dB and 8 dB, respectively.

TABLE 16. Received RF power vs tone and carrier frequency.

TX GUI config.	Received Power Tone [dBm]			
	10 MHz	100 MHz	250 MHz	350 MHz
(57.24, 0)	-73.4	-68.56	-73.04	-73.1
(59.4, 0)	-73.12	-67.55	-72.47	-72.63
(61.56, 0)	-74.96	-71.50	-75.26	-75.32
(63.72, 0)	-79.49	-75.45	-80.34	-79.75
(57.24, 8)	-81.73	-73.61	-82.77	-82.17
(59.4, 8)	-80.39	-74.35	-82.4	-82.4
(61.56, 8)	-84.17	-76.95	-85.14	-84.77
(63.72, 8)	-88.59	-81.71	-90.69	-89.84
(57.24, 20)	-99.15	-92.98	-100.73	-100.33
(59.4, 20)	-98.86	-96.43	-101.71	-102.06
(61.56, 20)	-101.04	-97.88	-103.78	-104.17
(63.72, 20)	-105.05	-101.93	-108.19	-107.9

TABLE 17. VUBIQ RX gain, considering TX IF_{Att} = 20 dB, and RX IF_{Att} set to either 0 dB or 8 dB.

Digital Att. [dB]	RX Gain [dB]
0	49.2
8	44.2

C. LOOP-BACK SYSTEM CHARACTERIZATION

1) OVERALL IF-IF FREQUENCY RESPONSE MAGNITUDE

In this section the transmitted to received (IF-IF) magnitude response, of the PEM009 is evaluated. The measurement setup block diagram similar to the one illustrated in Fig.17, whereas both input and outputs of the RF front-end are directly connected to the VNA simultaneously. Results of the transceiver FR are illustrated in Fig. 18, for f_C = 60.48 GHz and TX IF_{Att} = 20 dB, for RX IF_{Att} values of 0, 8, 12 and 20 dB.

From 18, it is verified that the PEM009 frequency magnitude response is not flat across its entire "announced" 1.2 GHz bandwidth. Instead, it has actually a shape similar to what is seen in a Low Pass Filter (LPF). According to the
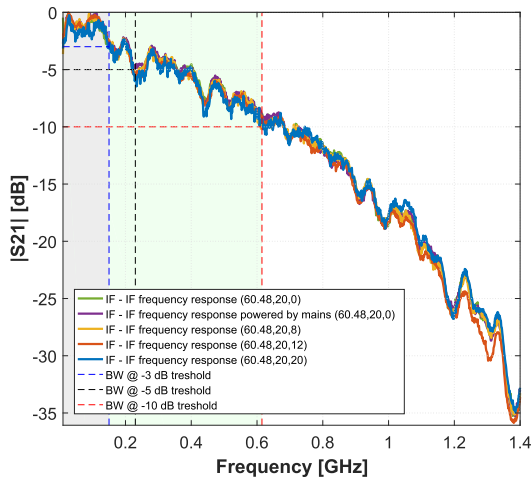
IEEE *Access*

R. Gomes *et al.*: Will COTS RF Front-Ends Really Cope With 5G Requirements at mmWave?

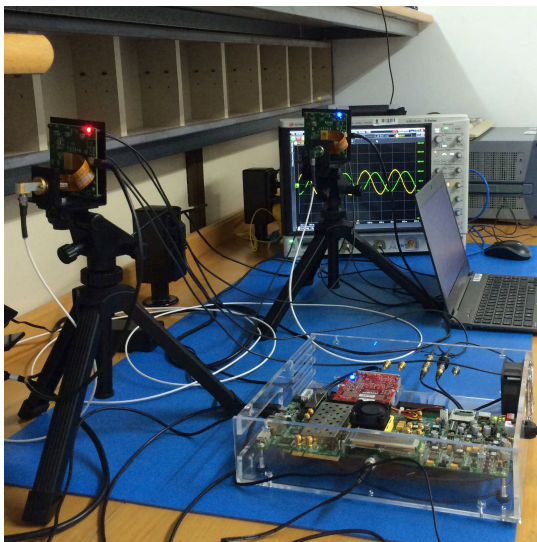**FIGURE 18.** PEM009 magnitude IF-IF response over its operation frequency range.

FIGURE 19. Picture of the IQ imbalances test bench measurement setup.

results, the effective 3 dB BW of the RF front-end is around 150 MHz (Δf_1). However, even considering a threshold level of 5 dB or 10 dB below, the BW increases to 230 MHz (Δf_2) and 615 MHz (Δf_3), respectively. As a rule of thumb, it is considered the 10 dB threshold, a reasonable trade-off between magnitude variation response versus BW.

2) IQ AND DC OFFSET IMBALANCES ASSESSMENT

In order to evaluate and characterize IQ imbalances introduced on baseband signals by the RF front-end, the following measurement process was conducted: SDR presented in section III was used to generate CW I/Q signals 90° out of phase and connected to the TX board. At the output of RX, both received I/Q signals are connected to the input ports of a 20 GSps wideband Keysight Technologies S-series oscilloscope, and remotely acquired by a host PC to be post-processed. A picture of the measure setup is shown in Fig. 19.

To calculate both phase and gain imbalances present in both I/Q captured signals, some mathematical considerations are needed. Firstly, amplitude imbalance is defined as [53]:

$$\alpha = 10 \log(1 + \frac{a_I - a_Q}{a_I + a_Q})[dB], \qquad (6)$$

where, a_I and a_Q, are the amplitude on I and Q branches, respectively. Secondly, phase imbalance (β) is calculated as:

$$\beta = 90 - \Delta\theta, \qquad (7)$$

where constant 90 represents the reference phase offset between both sine (I) and cosine (Q) waveforms, and $\Delta\theta$ is phase difference between both received branches, which ideally is 90°.

The DC voltage offset is calculated processing the same data used in the IQ imbalances assessment. The obtained results are summarized in Fig. 20, considering f_C equals to 60.48 GHz, and TX/RX $IF_{Att} = 17.3$ dB.
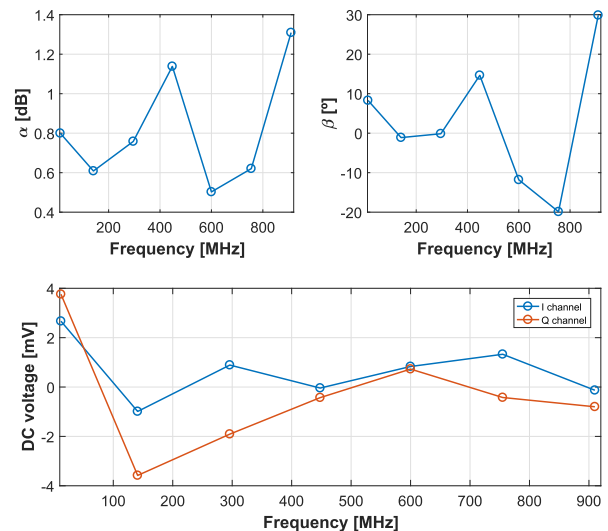

FIGURE 20. Results for PEM009 imbalances: a) gain; b) phase and c) DC voltage offset over its frequency range.

3) CARRIER FREQUENCY OFFSET AND DEMODULATOR FREQUENCY STABILITY

In previous measurement sections, the same clock reference source was used on both TX and RX devices, to avoid additional distortions effects from CFO. However, in a realistic environment, both TX and RX must be operating with independent clock sources, and thus CFO is always present. In order to assess this phenomena on the PEM009, two clock boards, as the one presented in Fig. 8, were used. The measurement setup is very similar to the one illustrated in Fig. 17, whereas a single tone (293 MHz) is transmitted instead, and each TX/RX device has their own independent clock source. At the received side, baseband signals are connected to a SA. The demodulated signal spectrum is used to measure both CFO value and the frequency stability of the RX. The measured signal FR is depicted in Fig. 21, where a
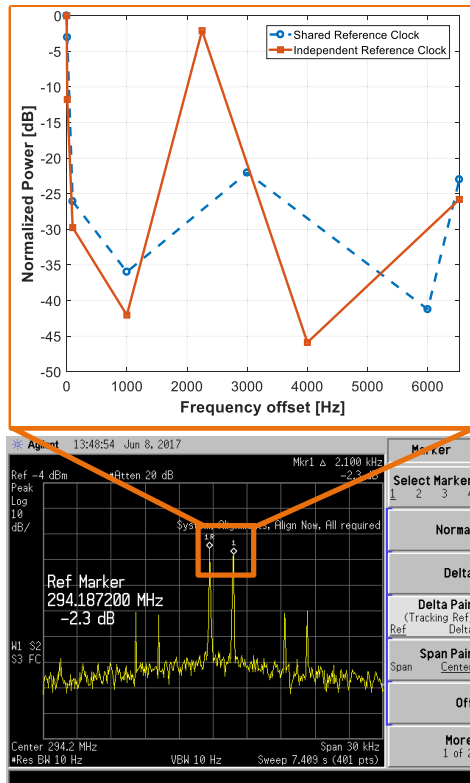
R. Gomes *et al.*: Will COTS RF Front-Ends Really Cope With 5G Requirements at mmWave?

IEEE *Access*

FIGURE 21. Results of PEM009 signal frequency stability assessment considering both shared and independent clock configurations.

TABLE 18. Relation between EVM, BER and digital modulation, according to [28].

BER [%]	Digital Modulation	EVM [dB]
10^{-3}	4-QAM	-10
	16-QAM	-17
	64-QAM	-24
	256-QAM	-32
10^{-4}	4-QAM	-12
	16-QAM	-19
	64-QAM	-26
	256-QAM	-34
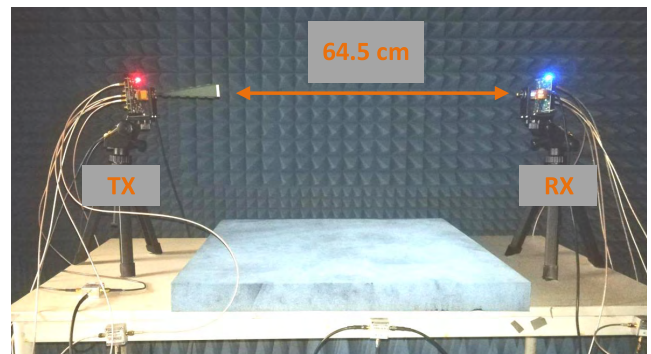
FIGURE 22. MmWave link employed for OFDM performance assessment (PEM009 as RF front-end).

replica of the demodulated signal spaced 2.2 kHz is visible. Additionally, other frequency spurious are verified in both shared and independent clock configurations. The minimum Spurious Free Dynamic Range (SFDR) values for both clock configurations, are approximately −21, and −24.7 dBc. This might be due to carrier modulation of TX IMD products, which will eventually appear at the RX baseband signal spectrum.

VI. IMPACT OF PEM009 NON-LINEARITIES ON OFDM TRANSMISSION PERFORMANCE

In this section, the effect of RF impairments on the quality of TRX OFDM system, presented in subsection III-B, over the air at 60 GHz, is evaluated and demonstrated for different conditions of RX SNIR, and for 4-, 16-QAM modulations. To reduce possible OFDM performance degradation due to multipath effect, transmission is established inside an anechoic chamber under Line-of-Sight (LOS) conditions. Hence, it is possible to accurately assess the impact of the RF front-end on a wireless mmWave OFDM communication system. The QoS is assessed through EVM, and spectral efficiency per stream analysis. BER is estimated using the relation between this metric and EVM, given in Table 18 [28]. The experimental setup is shown in Fig. 22, where both TX/RX wave-guide devices are connected to 25 and 0 dBi horn antennas, respectively, and spaced 64.5 cm apart (enough distance to avoid saturation of the RX LNA

(Low Noise Amplifier)). In addition, VUBIQ RF IF settings were set to 20 dB in both TX/RX devices, and the center carrier frequency set to 60.48 GHz, in order to mitigate the presence of non-linearities, as it was verified in the results from the previous section.

EVM results have been computed for each OFDM IF modulated signal under different SNIR and with either the presence or absence of CFO. For example, Table 19 shows the measured average EVM values ($\overline{EVM}$), from three ILA samples acquisition, for an IF OFDM modulated signal at 312.5 MHz (IF4). The minimum average EVM value, −14.34 dB, is verified for an input power of −16.72 dBm when both TX/RX devices are clocked using the same source. For a subjective quality assessment metric of this EVM value, 4- and 16-QAM received constellations, are depicted in both Fig. 25a and Fig. 25b, respectively. While, for the 4-QAM constellation the scatter points are well separated, in the 16-QAM a relatively high distortion of the received scatter symbols is clearly visible, since they are quite close from each other, therefore indicating that it is very likely to obtain erroneous decoded data. Additionally, when both TX and RX are either operating independently or using I and Q branches, the performance degradation is very severe. This is, data is not even successfully decoded for 4-QAM ($EVM > −2$ dB). Results for remaining IF values are summarized in Fig. 23a. From such results, average EVM is always below the target −10 dB for a 4-QAM BER lower than 10^{-3}, for all

IEEE Access

R. Gomes *et al.*: Will COTS RF Front-Ends Really Cope With 5G Requirements at mmWave?

TABLE 19. SNIR vs EVM results using IF4 OFDM modulation for both shared and independent clock configurations, for PEM009.

Gain Sel.	Analogue* Att. [dB]	TX Input Power [dBm]	Analogue RX SNIR [dB]	$\overline{EVM}^{\dagger}$ [%]	[dB]	$\overline{EVM}^{\ddagger}$ [%]	[dB]	$\overline{EVM}^{\dagger\dagger}$ [%]	[dB]
0	0	-25.63	26.46	32.06	-9.85	143.44	3.75	72.62	-2.71
	5	-30.63	20.74	64.87	-3.66	160.64	4.51	-§	-§
	10	-35.63	14.80	134.60	2.61	201.21	6.26	-§	-§
1	0	-19.76	25.64	27.30	-11.24	100.84	1.16	78.67	-2.04
	5	-24.76	28.65	55.98	-4.79	124.23	2.99	-§	-§
	10	-29.76	24.76	78.34	-2.06	163.30	4.75	-§	-§
2	0	-17.83	20.30	29.33	-10.63	97.54	0.99	75.49	-2.23
	5	-22.83	27.43	31.92	-5.89	120.47	2.35	-§	-§
	10	-27.83	26.27	50.74	-5.89	102.47	1.42	-§	-§
3	0	-16.21	17.03	22.66	-12.77	63.63	-2.92	72.75	-2.65
	5	-21.21	22.47	23.54	-12.06	83.65	-0.96	-§	-§
	10	-26.21	30.92	31.26	-9.80	137.71	3.57	-§	-§
4	0	-14.83	16.48	24.61	-12.02	100.02	0.71	70.72	-2.88
	5	-19.83	21.06	25.27	-11.79	87.77	0.12	-§	-§
	10	-24.83	30.06	52.20	-5.11	100.59	0.98	-§	-§
5	0	-13.64	16.55	23.88	-12.05	84.95	-0.46	67.86	-3.22
	5	-18.64	18.42	26.25	-11.79	85.21	-0.05	-§	-§
	10	-23.64	28.20	34.74	-8.70	102.14	1.13	-§	-§
6	0	-12.62	17.47	23.13	-12.66	97.24	0.77	72.34	-2.65
	5	-17.62	18.20	28.99	-10.41	113.84	1.94	-§	-§
	10	-22.62	26.41	33.26	-9.11	106.82	1.38	-§	-§
7	0	-11.72	17.07	26.19	-11.61	93.91	0.79	74.73	-2.42
	5	-16.72	**26.35**	**19.01**	**-14.34**	109.36	1.65	-§	-§
	10	-21.72	23.70	31.69	-9.52	88.48	0.94	-§	-§

(*) Variable attenuator placed between the SDR and transmitter.

($\dagger$) Shared clock source configuration.

($\ddagger$) Independent clock source configuration.

($\dagger\dagger$) IQ configuration with shared clock source.

($\S$) Not considered.

IF values. Consequently, average EVM performance degradation results of a mmWave transmission using PEM009, for all IF values, are shown in Fig. 23b. This EVM degradation is the EVM difference when using IF back-to-back and using mmWave PEM009 chip-set. A minimum degradation value of 27.17 dB, 18.17 %, is achieved for $IF = 312.5$ MHz. For this best case scenario, it is possible to estimate the TX input power operating range. According to Fig. 24, such range is approximately 10 dB, which means RF front-end system ensures a relatively good performance for TX input power between $[-26.5, -16.5]$ dBm (considering an EVM threshold of -10 dB).

VII. REFERENCE RF FRONT-END
As it has been verified in section VI, analogue upconversion/downconversion stages presented in PEM009 induce a severe performance degradation on OFDM communications. This led authors to design and develop a more academic RF front-end approach as reference, herein designated Instituto de Telecomunicações (IT) RF front-end. Such device is composed of several connectorized HXI analogue components rather than a COTS chip-set approach. This alternative is intended to provide a multi-Gibabit/s radio in-the-loop at mmWave frequencies for future wireless communications prototypes, such as 5G. Effectively, even if a 2 GHz channel in the 60 GHz band is used to transmit data employing both 4-QAM, and 16-QAM modulations, data-rate would still be limited to 4, and 8 Gbps, respectively. Therefore, there is demand for improving both system reliability and data-rates (over 10 Gbps is the target for 5G). In this context, an architecture overview, and system performance of IT RF front-end are presented in this section.

A. ARCHITECTURE OVERVIEW
At the TX, it has been considered a typical direct-conversion (in order to avoid IQ imbalance effects on transmitted signals), also known as, homodyne architecture. It is composed by a PLL operating at 15 GHz, a $4X$ multiplier, which brings the LO signal to 60 GHz, and a upconversion mixer. Also, an external 10 MHz reference clock is required for the PLL. The block diagram of the transmitter, as well as, the specification of each analogue component is illustrated in fig. 26. Moreover, in order to reduce the presence of PA non-linearities, a amplification stage at 60 GHz is not considered.
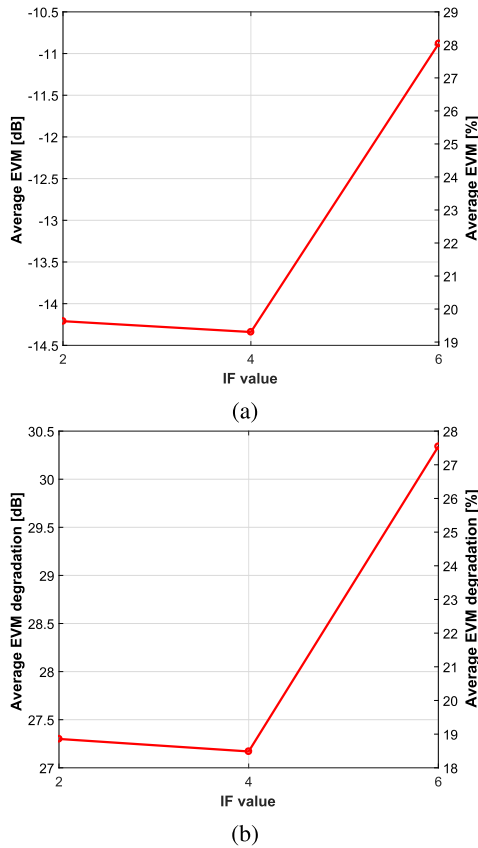
R. Gomes *et al.*: Will COTS RF Front-Ends Really Cope With 5G Requirements at mmWave?

IEEE *Access*

(a)

(b)

FIGURE 23. Results of EVM: a) performance, and b) degradation, considering PEM009.
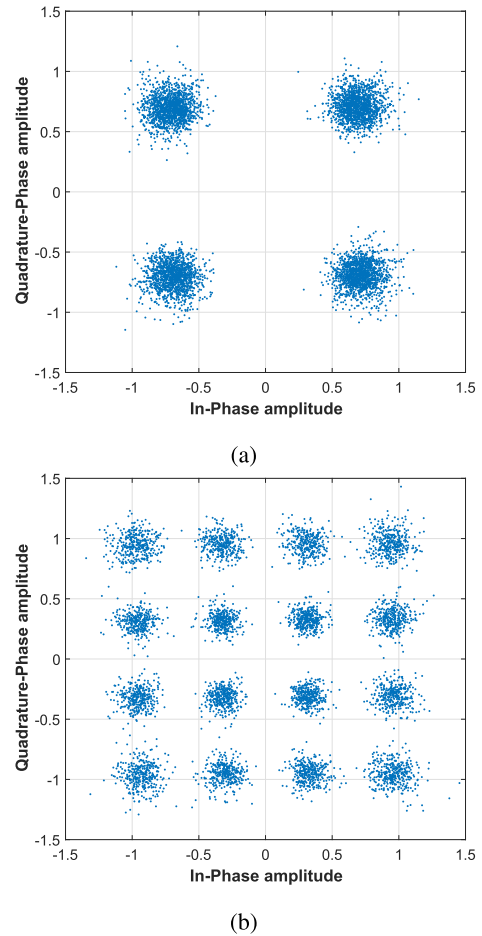

(a)

(b)

FIGURE 25. Received scatter constellation plots for: a) 4-QAM, and b) 16-QAM, considering an IF4 OFDM power transmission of −16.72 dBm on the PEM009 TX.
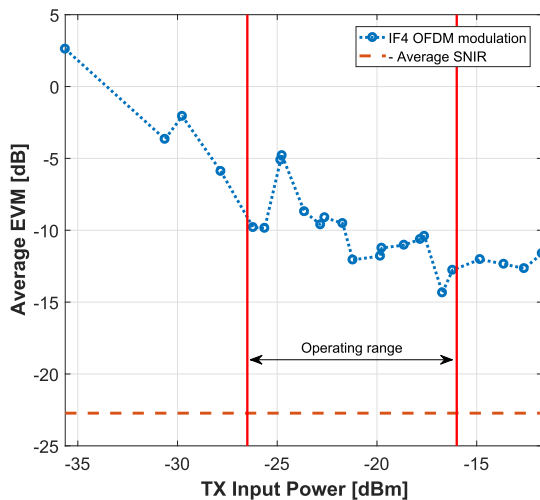

FIGURE 24. PEM009 input power versus EVM, for IF4 OFDM with absence of CFO.

FIGURE 26. IT homodyne architecture transmitter.

Regarding the receiver, a two stage heterodyne architecture is employed. An LNA is used to amplify received signals, followed by a downconversion to a 6 GHz IF stage, performed trough a first mixing process with a 54 GHz LO signal. In a second downconversion stage, received signals are brought to baseband/low IF frequencies.
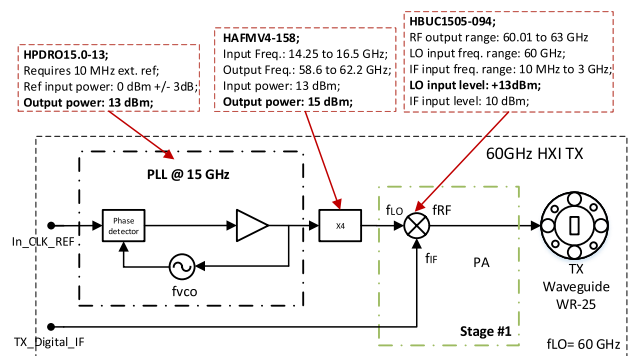
Therefore, unlike the transmission architecture, two PLLs operating at 13.5 and 6 GHz are needed in this one, as it can be seen in Fig. 27.

Furthermore, the external clock references for both TX/RX PLLs are generated by a PRS10M rubidium oscillator. Such reference clock signals are characterized by very low phase noise, as verified in Table 20, and very high frequency stability (≈0.05ppb), being, therefore, very
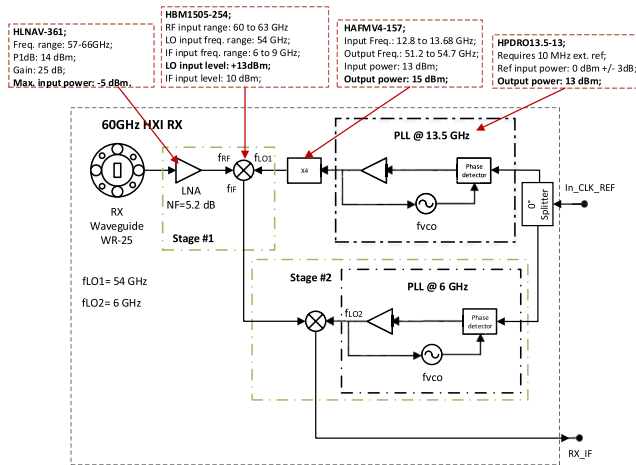
IEEE *Access*

R. Gomes *et al.*: Will COTS RF Front-Ends Really Cope With 5G Requirements at mmWave?

FIGURE 27. IT two-step superheterodyne architecture receiver.

TABLE 20. Measured PN of the rubidium oscillator signal.

Freq. Offset [Hz]	Phase Noise [dBc/Hz]
10	-78
100	-80
1000	-81
10000	-100
100000	-122
1000000	-128

FIGURE 28. Results of IT signal frequency stability assessment considering both shared and independent clock configurations.

FIGURE 29. MmWave link used for OFDM performance assessment, using IT RF front-end.

reliable clock sources. Moreover, in an independent clock configuration between TX/RX (presence of CFO), two rubidium oscillators were also considered. Fig. 28, shows, not only stability of the analogue demodulator when a CW signal is transmitted, but also the presence of very low power spurious for both shared and independent clock sources configurations. In fact, unlike the PEM009, no significant spectrum difference is noticed between both clock configurations. In addition, CFO is negligible when IT RF front-end is operating with independent clock sources.

B. OVER THE AIR OFDM SYSTEM PERFORMANCE

Similarly to what has been presented for the PEM009 system, the effect of RF impairments on the quality of OFDM transmission over the air using IT RF front-end, is evaluated for different SNIR conditions at the receiver. The corresponding measurement setup, presented in Fig. 29, is very similar to the one presented in section VI. The propagation environment and scenarios are also the same. However, due to the lack of a PA at the TX, 25 dBi antennas have been employed at both TX/RX terminals, increasing the system usable distance range to 74.5 cm. Again, QoS is assessed through EVM, BER, and digital modulation analysis.

Average EVM results under different conditions of SNIR have been summarized in Table 21, for IF4 OFDM transmissions. Comparing these results with the ones obtained in section V for PEM009, it is clearly seen that IT RF front-end
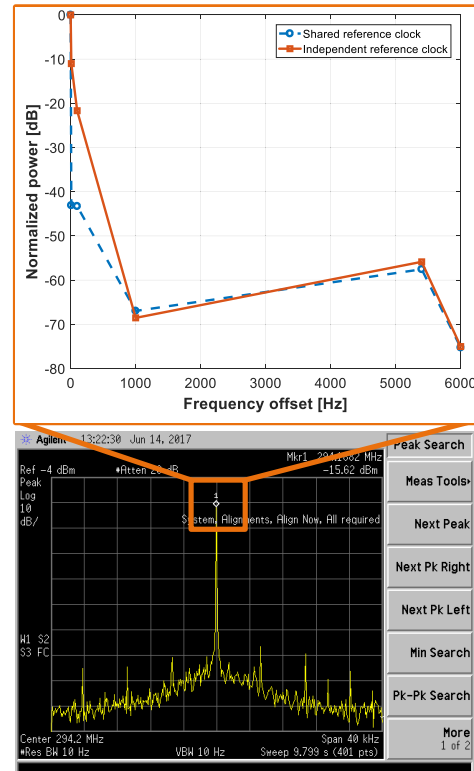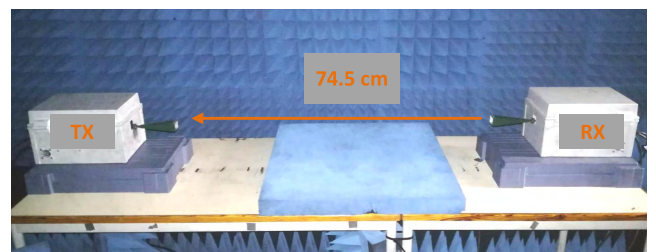
induces much less RF impairments in the OFDM system than PEM009. Minimum obtained average EVM is now −32.58 dB, significantly better than the −14.34 dB verified for the VUBIQ system. Fig. 30, shows the input power operating range of the IT RF front-end considering IF4, where it is clearly seen that such system operates also in a wider input dynamic power range, leading to an excess of approximately 11 dB when compared with the PEM009. Results presented in Fig. 31, for an EVM of −32.58 dB, indicate that this RF front-end can handle QAM modulations up to 256-QAM, against the 16-QAM verified for the PEM009. This leads to an increased data-rate of 100%, and thus, the mmWave OFDM communication system is now able to provide 1 Gbps of data transmission. Moreover, in Figs. 32a and 32b it is shown the minimum average EVM and its degradation for the remaining IF OFDM modulations. For IF values of

R. Gomes *et al.*: Will COTS RF Front-Ends Really Cope With 5G Requirements at mmWave?

IEEE*Access*

TABLE 21. SNIR vs EVM results using IF4 OFDM modulation for both shared and independent clock configurations, for IT RF front-end.

Gain Sel.	Analogue* Att. [dB]	TX Input Power [dBm]	Analogue RX SNIR [dB]	$\overline{EVM}^{\dagger}$ [%]	$\overline{EVM}^{\dagger}$ [dB]	$\overline{EVM}^{\ddagger}$ [%]	$\overline{EVM}^{\ddagger}$ [dB]
0	0	-25.63	28.70	6.83	-23.30	5.40	-25.34
	5	-30.63	22.90	11.56	-18.74	9.43	-20.51
	10	-35.63	18.80	20.57	-13.73	16.50	-15.65
1	0	-19.76	33.79	3.67	-28.72	3.01	-30.42
	5	-24.76	29.78	5.75	-24.81	4.79	-26.39
	10	-29.76	24.06	10.49	-19.58	8.28	-21.64
2	0	-17.83	36.00	3.11	-30.13	2.62	-31.60
	5	-22.83	31.00	4.87	-26.26	3.96	-28.05
	10	-27.83	25.19	8.48	-21.45	6.67	-23.52
3	0	-16.21	36.67	2.74	-31.21	2.30	-32.52
	5	-21.21	32.42	4.40	-27.12	3.37	-29.43
	10	-26.21	26.74	7.14	-22.93	5.64	-24.98
4	0	-14.83	**37.81**	**2.35**	**-32.58**	2.23	-32.99
	5	-19.83	34.00	3.44	-29.27	3.00	-30.44
	10	-24.83	29.30	6.04	-24.38	4.81	-26.36
5	0	-13.64	38.48	2.50	-32.36	2.31	-32.70
	5	-18.64	34.22	3.08	-30.22	2.84	-30.93
	10	-23.64	29.96	5.05	-25.94	4.45	-26.98
6	0	-12.62	38.08	2.69	-31.36	2.26	-32.87
	5	-17.62	34.00	3.07	-30.15	2.57	-31.78
	10	-22.62	31.42	4.57	-26.80	3.95	-28.06
7	0	-11.72	39.00	2.55	-31.87	2.37	-32.46
	5	-16.72	36.02	2.58	-31.75	2.37	-32.48
	10	-21.72	32.63	4.06	-27.82	3.64	-28.77

(*) Variable attenuator placed between the SDR and transmitter.

($\dagger$) Shared clock source configuration.

($\ddagger$) Independent clock source configuration.

TABLE 22. Minimum received power at RX vs digital modulation, using IT RF Front-End.

| Digital Modulation	Minimum received Power [dBm]
4-QAM	-84.09
16-QAM	-66.65
64-QAM	-59.09
256-QAM	-48.35

312.5 and 468.75 MHz, EVM is below 3 %, representing a performance degradation below 2% when compared to a back-to-back configuration. This is quite remarkable, since the EVM values at 60 GHz are lower than the 2.5 % required by sub-6 GHz WiFi (IEEE 802.11.ac) to employ 256-QAM OFDM transmissions [54]. To the best of the authors' knowledge, this spectral efficiency per stream and SNR results go significantly beyond the state-of-the-art, when compared to the current mmWave testbeds presented in table 2. Finally, for the proposed link budget the received power versus digital modulation, for an BER of 10^{-3}, is presented in Table 22.
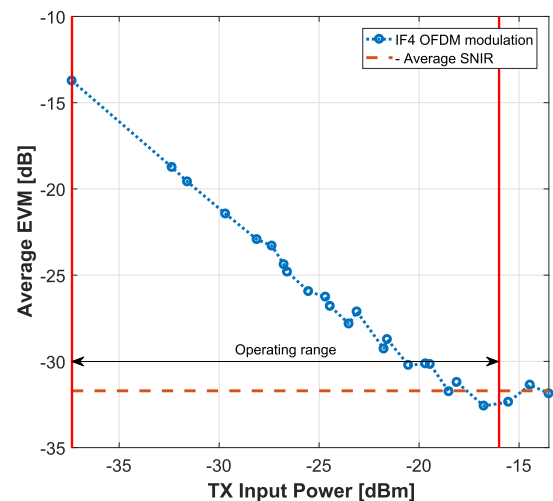
FIGURE 30. IT RF front-end input power versus EVM, for IF4 OFDM with absence of CFO.

VIII. MMWAVE EVM LINK BUDGET

It is well known that OFDM performance is inherently dependent on the SNR present, which can be easily measured using

IEEE *Access*

R. Gomes *et al.*: Will COTS RF Front-Ends Really Cope With 5G Requirements at mmWave?
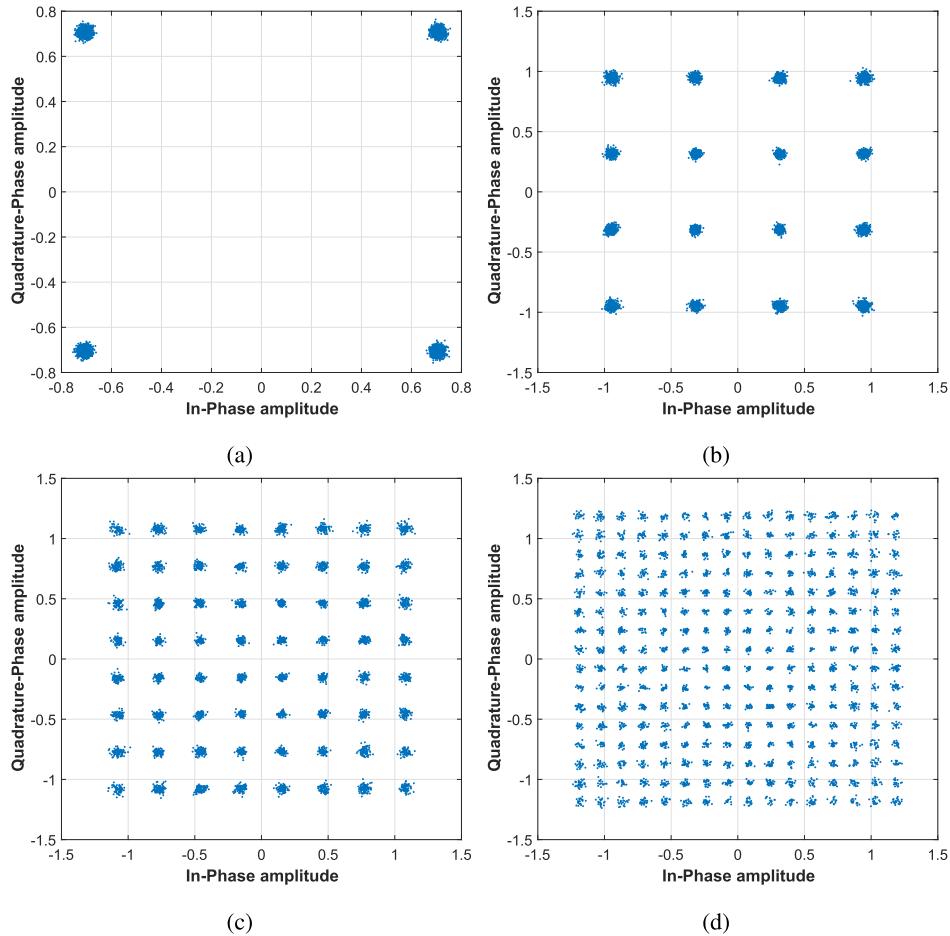
FIGURE 31. Received scatter constellation plots for: a) 4-QAM, b) 16-QAM, c) 64-QAM, d) 256-QAM, considering an IF4 OFDM power transmission of −14.83 dBm on the IT RF front-end.

a spectrum analyzer placed at the receiver. To this extent, SNR and EVM metrics can be related by (8) [55]. However that is only verified in the absence of any RF impairments. Therefore, in order to assess the maximum radio link range, for a certain performance threshold, the RX EVM must be accurately estimated. For example, as it is illustrated in Fig. 33, PA in-band intermodulation products can significantly reduce this ratio. Hence, such impairment is characterized by the SNIR ratio instead, and is mainly caused by the PA saturation power level, which can be assessed following the proposed method described in section V. On the other hand, PN from 60 GHz local oscillators can also play a very important role on the overall mmWave system performance. Despite the fact that this impairment does not contribute to the SNIR, its impact might result in severe EVM degradation. In order to evaluate this, PN must be accurately measured, modeled and its individual impact on the OFDM system performance assessed through measurement.

$$\overline{\text{EVM}}_{RMS} \approx \sqrt{\frac{1}{SNR}} \Leftrightarrow$$
$$\Leftrightarrow \overline{\text{EVM}}|_{dB} \approx -SNR|_{dB}. \qquad (8)$$

A. 60 GHZ LO'S PN MEASURE, MODELING AND PERFORMANCE DEGRADATION EFFECT ON OFDM SYSTEMS

In order to assess the individual PN effect on OFDM systems, the measurement setup depicted in Fig. 34 must be considered, where the rubidium clock is used as reference signal to both ADC/DAC sample clock rate. In addition to all DSP algorithms presented in the proposed SDR (see Fig. 1), a phase noise generator source was included in the receiver OFDM chain. The PN generator was implemented according to [56], and based on the 60 GHz measured PN values, of both RF front-ends, presented in Fig. 35a. To validate this algorithm, Power Spectral Density (PSD) comparison of real-time generated noise samples with the average measured values were performed. As it can be verified from Fig. 35b, a good match between both modeled and measured curves is obtained, in particular for both PEM009 and IT RF front-ends.

Measured EVM results versus modeled PN for each source, is presented in Table 23. In this table, the performance degradation is characterized in terms of $\triangle EVM$, which is the difference between measured $\overline{EVM}$ in the presence and
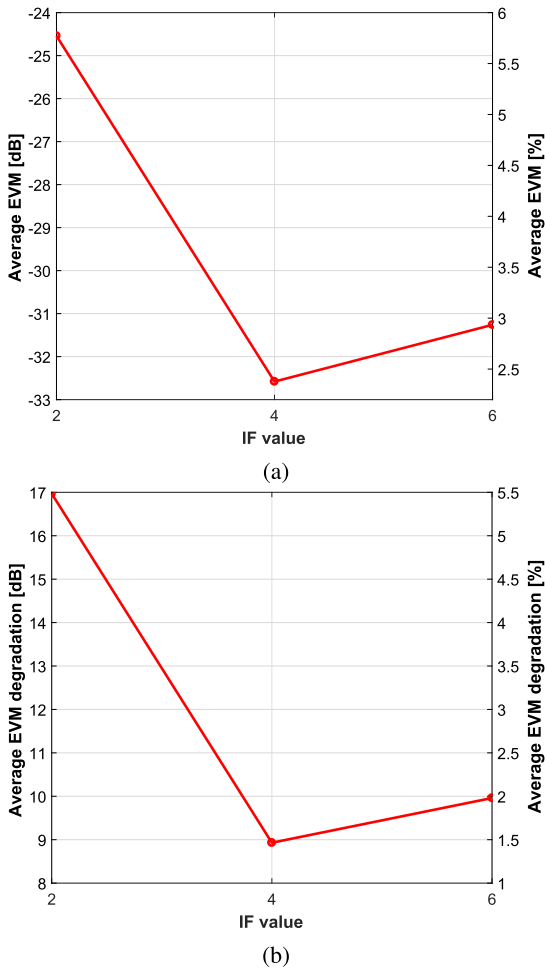
R. Gomes *et al.*: Will COTS RF Front-Ends Really Cope With 5G Requirements at mmWave?

IEEE *Access*

FIGURE 32. Results of EVM: a) performance, and b) degradation, considering IT RF front-end.

FIGURE 33. Illustration of the SNIR metric.

FIGURE 34. Block diagram of the PN assessment setup.

FIGURE 35. PSD comparison of a) measured PN curves from both M6300 and Rubidium oscillators with both 60 GHz RF front-ends, and b) generated PN modeling curves for both IT and VUBIQ PEM009 systems, with their PN measurements curve values.
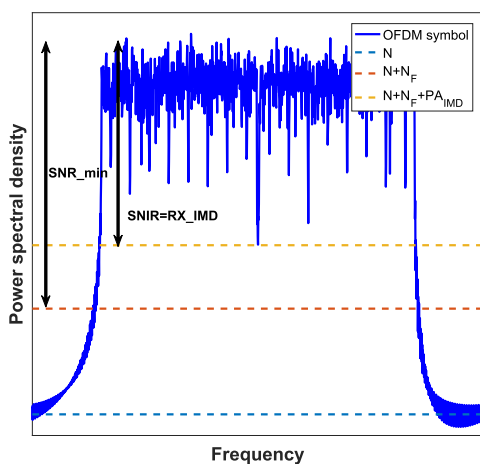
absence of PN from the mmWave LO. Two additional PN sources are modeled and presented in Fig. 35a (curves A and B) to assess different PNs' impact on OFDM's EVM performance. These results show that PN noise has a significant
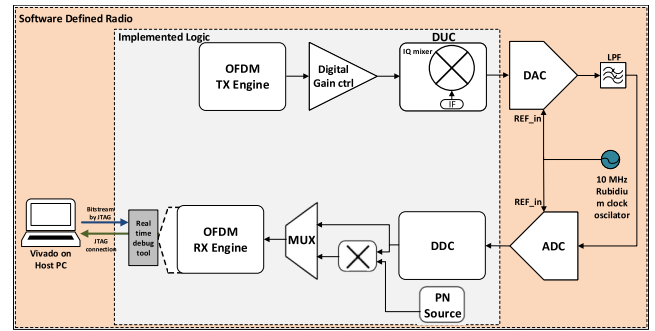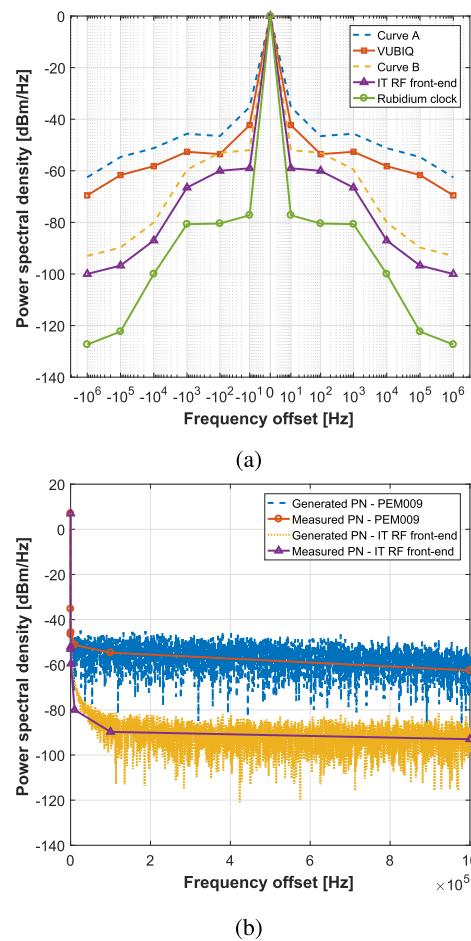
impact on the OFDM EVM performance. That is, when PN model is not implemented, $\overline{SNR} = -\overline{EVM}$ [dB], which is in agreement with (8), while $|\overline{EVM}| = \overline{SNR} - 9$ and $|\overline{EVM}| = \overline{SNR} - 23$, when IT and VUBIQ PEM009 RF front-ends are considered, respectively. This is in line with the results from Table 21, when $SNIR = 37.81$ dB yielded an average EVM of -32.58 dB, when using IT's RF system. These results also show that OFDM degradation performance is more relevant

IEEE Access

R. Gomes *et al.*: Will COTS RF Front-Ends Really Cope With 5G Requirements at mmWave?

TABLE 23. EVM performance degradation values for VUBIQ PEM009 and IT reference RF front-end PN curves.

PN curve source	$\overline{SNR}$ [dB]	$\overline{EVM}$ [dB]	$\triangle EVM$ [dB]
No PN (baseband only)		-42	N/A
IT RF model		-33	9
Curve B	42	-31.6	10.4
VUBIQ PEM009 model		-19	23
Curve A		-14.4	27.6

when considering the VUBIQ PEM009's, which is explained by its higher PN PSD values versus frequency offset, when compared to the IT's one.

B. PROPOSED METHOD

As it was verified in the previous subsection, a measured high SNR values does not always translate into good system performance. Therefore, minimum SNR, SNR_{min}, value must be accurately estimated for a certain EVM value, in order to properly manage the TX power. In other words, optimum SNR value must be estimated based on the maximum system's performance in terms of EVM. In this context, the following practical EVM link budget formulation, which takes into account both PA and PN impairments, is proposed.

1) $SNR_{min} = |EVM_{PN}|$, where EVM_{PN} is the average EVM floor value of the system performance under PN conditions;
2) Since 1) is just verified if $RX_{IMD} > |EVM_{PN}|$, where RX_{IMD} is the power difference between the fundamental tone with the IMD product, an additional margin should be considered to mitigate the PA non-linearities. Therefore, $SNR_{min} \geq |EVM_{PN}| + IR_{IMD}$, where IR_{IMD} is the third order IMD power-to-noise ratio.

Moreover, since the EVM versus PN measurement indicated in the previous subsection could be impractical in same RF systems, such can be estimated from the following mathematical equation (9), obtained from polynomial curve fitting.

$$\overline{EVM}(PSD_0) = 0.01343.PSD_0^2 + 2.511.PSD_0 + 73.12, \tag{9}$$

where, PSD_0 is the PSD of PN at 1kHz. This allows the calculation of average EVM for PSD values from -80.7 up to -45.6 dBm/Hz at 1kHz of CFO, and has been extrapolated from Fig.36.

Moreover, the maximum separation between terminals (d_{max}) of a system in presence of the joint effect of both PA and PN impairments, considering the estimated SNR_{min}, can be expressed by (10) [57].

$$\begin{cases} L_{PL} = P_{TX_{BB}} + G_{RF_{TX}} + G_{AntTX} - SNR_{min} \\ \quad + G_{AntRX} + G_{RF_{RX}} - IL[dB] \\ d_{max} = 10^{(L_{PL}-L_{PL_o})/10n} [m], \end{cases} \tag{10}$$
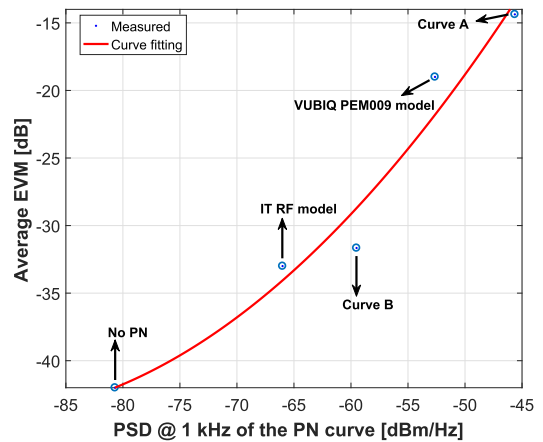
FIGURE 36. $\overline{EVM}$ with PN PSD @ 1 kHz ($\overline{SNR}$ = 42 dB).

where, $P_{TX_{BB}}$ is the baseband output power, both $G_{RF_{TX}}$, and $G_{RF_{RX}}$, are the TX/RX RF front-end gain, respectively, G_{AntTX}, and G_{AntRX} are the TX/RX antenna gain, respectively, and IL is the implementation loss. The path loss is represented by L_{PL}. The L_{PL_o} is the path loss at $d_0 = 1m$, and n is the path loss exponent.

IX. CONCLUSION

In this paper, a study on the impact of RF impairments in a complete multi-Gigabit/s radio in-the-loop OFDM mm-wave communication system, implemented according to the LTE advanced, for high data-rate applications, and considering 4-, 16-, 64-, 256-QAM, was presented for both COTS and reference (IT) RF front-ends. Additionally, PEM009 system measurements for: PN characteristic curve, TX output power and gain, TX/RX IMD products, TX RF carrier and side-band leakages, RX clock leakage, RX sensitivity and gain, IQ imbalances, DC offset, bandwidth and finally CFO, were evaluated. The performance assessment of the OFDM system was conducted through EVM, BER, and spectral efficiency per stream analysis, considering a real-time transmission of pseudo-random bits over LOS radio channels located inside anechoic chamber.

It has been shown through an extensive measurement campaign, in particular, for the PEM009 RF front-end, that the most significant spurious frequency from TX/RX IMD products are about 39.35 and 35 dB below the desired tone, respectively. Both minimum carrier suppression, and side-band leakages values are in average 11 dBc, and -1.6 dBc, which means, mutual interference between adjacent TX channels will occur. Moreover, the carrier frequency of 60.48 GHz is the only option which ensures no significant clock leakages from the PLL circuit into both I/Q baseband channels. Consequently, considering this f_C, both IQ imbalances and DC offset impairments are very significant, and also both are frequency dependent. Finally, the available PEM009 RF front-end bandwidth considering a -3 dB threshold was found to be approximately 150 MHz.

R. Gomes *et al.*: Will COTS RF Front-Ends Really Cope With 5G Requirements at mmWave?

IEEE *Access*

However, typical OFDM systems might handle FR attenuations up to 10 dB and, consequently its bandwidth is increased to 625 MHz.

It has also been concluded that PEM009 fails to provide a reliable TX/RX independent end-to-end communication, since the CFO replica present in the received baseband channels leads to severe signal interference and therefore data is not successfully demodulated (relatively high EVM). However, authors believe that employing a LVPECL clock waveform type with the same measured PN of the rubidium signal, such issue would be overcome. Therefore, PEM009 in the presented configuration should only be used with a shared clock. Nevertheless, the spectral efficiency of the system is relatively low. For example, even considering its measured BW (615 MHz), the data-rate would still be limited to 2.5 Gbps, consequently failing to meet the 5G requirements. On the other hand, IT Front-end has proven to be a reliable choice, being able to provide a data-rate up to 16 Gbps, when employing 256-QAM (considering a 2 GHz channel). In fact, the usage of mmWave frequencies to transmit data has been demystified, since the possibility of having a 60 GHz link with the same EVM requirement of WiFi at 2.4 GHz was demonstrated.

Furthermore, it has been demonstrated that IQ imbalances induce the largest performance degradation in the OFDM waveform, when using the PEM009 RF front-end. In fact, this is line with the performed RF measurements, where it has been shown that such impairment is not only significant (max 1.4 dB, and 30° of both amplitude and phase distortion), that is also frequency dependent over the RF front-end bandwidth. Anticipating this, the authors have implemented the IQ mixing process in the digital domain, and the uncoded OFDM performance in terms of average EVM has been decreased from -2 dB to -14 dB, with BER below 10^{-3}. In addition, in absence of this impairment (IF OFDM transmission), the phase-noise effect turns out to be main limiting factor. In other words, it is dictating the overall system EVM floor value. This has also been validated by the implementation of a PN model in the receiver chain of the OFDM FPGA design, where such model was modulated from both PN characteristic curve values from both PEM009 and the IT RF front-end at 60 GHz. For example, in the PEM009 system, despite the presence of a SNR of 42 dB at RX, the minimum average EVM value is only -19 dB, yielding to an EVM degradation of 23 dB. This is the main reason why IT RF front-end outperforms the PEM009 performance (only 9 dB of EVM degradation due to PN), and thus enables modulation orders up to 256-QAM.

Results presented in this work also demonstrate that RF impairments from analogue upconversion/downconversion stages are the most restrictive factor in mmWave transmissions, limiting both data-rate and spectral efficiency. Therefore, currently COTS CMOS-based RF front-end technology is not ready yet to tackle 5G communication requirements, and must be evolved. While non-linearites from PA and PN can be compensated by backing off the PA input power,

and choosing a very stable LO, IQ imbalances should be completely mitigated by performing the IQ mixing process in the digital domain. This also avoids transmission of both image signal and RF carrier, from the output of the RF front-end. Finally, this work might be an important guide to establish mmWave real-time OFDM links meeting 5G requirements. In this context, a practical link budget formulation for accurate EVM estimation based on the presented mmWave RF measurements, is proposed.

REFERENCES

[1] Z. Pi and F. Khan, "An introduction to millimeter-wave mobile broadband systems," *IEEE Commun. Mag.*, vol. 49, no. 6, pp. 101–107, Jun. 2011.

[2] *LTE Advanced*. Accessed: Sep. 18, 2017. [Online]. Available: http://www.3gpp.org/technologies/keywords-acronyms/97-lte-advanced

[3] T. S. Rappaport, J. N. Murdock, and F. Gutierrez, Jr., "State of the art in 60-GHz integrated circuits and systems for wireless communications," *Proc. IEEE*, vol. 99, no. 8, pp. 1390–1436, Aug. 2011.

[4] Cisco Public, "Cisco visual networking index: forecast and methodology, 2016–2021," Cisco, San Jose, CA, USA, White Paper C11-481360-01, 2017.

[5] T. S. Rappaport *et al.*, "Millimeter wave mobile communications for 5G cellular: It will work!" *IEEE Access*, vol. 1, pp. 335–349, May 2013.

[6] *Everything You Need to Know About 5G*. Accessed: Sep. 18, 2017. [Online]. Available: http://spectrum.ieee.org/video/telecom/wireless/ everything-you-need-to-know-about-5g

[7] R. C. Daniels and R. W. Heath, "60 GHz wireless communications: Emerging requirements and design recommendations," *IEEE Veh. Technol. Mag.*, vol. 2, no. 3, pp. 41–50, Sep. 2007.

[8] J. Kim, J.-J. Lee, and W. Lee, "Strategic control of 60?GHz millimeter-wave high-speed wireless links for distributed virtual reality platforms," *Mobile Inf. Syst.*, vol. 2017, Mar. 2017, Art. no. 5040347, doi: 10.1155/2017/5040347.

[9] J. G. Andrews *et al.*, "What will 5G be?" *IEEE J. Sel. Areas Commun.*, vol. 32, no. 6, pp. 1065–1082, Jun. 2014.

[10] G. Wunder *et al.*, "5GNOW: Non-orthogonal, asynchronous waveforms for future mobile applications," *IEEE Commun. Mag.*, vol. 52, no. 2, pp. 97–105, Feb. 2014.

[11] D. Soldani and A. Manzalini, "Horizon 2020 and beyond: On the 5G operating system for a true digital society," *IEEE Veh. Technol. Mag.*, vol. 10, no. 1, pp. 32–42, Mar. 2015.

[12] P. Demestichas *et al.*, "5G on the horizon: Key challenges for the radio-access network," *IEEE Veh. Technol. Mag.*, vol. 8, no. 3, pp. 47–53, Sep. 2013.

[13] G. Consortium, "5G waveform candidate selection derivable 3.1," *5GNOW*, vol. 2013, no. 1, pp. 1–110, Nov. 2013.

[14] *Understanding 5G: Perspectives on Future Technological Advancements in Mobile*, GSMA Intell., London, U.K., 2014.

[15] H. Yang, P. F. M. Smulders, and M. H. A. J. Herben, "Indoor channel measurements and analysis in the frequency bands 2 GHz and 60 GHz," in *Proc. IEEE 16th Int. Symp. Pers., Indoor Mobile Radio Commun.*, vol. 1, Sep. 2005, pp. 579–583.

[16] F. Wu, Y. Li, and M. Zhao, "Estimation of TX I/Q imbalance at the RX side with RX I/Q imbalance and carrier frequency offset for OFDM systems," in *Proc. IEEE Globecom Workshops (GC Wkshps)*, Dec. 2014, pp. 960–965.

[17] P. Smulders, "Exploiting the 60 GHz band for local wireless multimedia access: Prospects and future directions," *IEEE Commun. Mag.*, vol. 40, no. 1, pp. 140–147, Jan. 2002.

[18] H. Xu, V. Kukshya, and T. S. Rappaport, "Spatial and temporal characteristics of 60-GHz indoor channels," *IEEE J. Sel. Areas Commun.*, vol. 20, no. 3, pp. 620–630, Apr. 2006, doi: 10.1109/49.995521.

[19] F. Gutierrez, S. Agarwal, K. Parrish, and T. S. Rappaport, "On-chip integrated antenna structures in CMOS for 60 GHz WPAN systems," *IEEE J. Solid-State Circuits*, vol. 27, no. 8, pp. 1367–1378, Oct. 2009.

[20] T. Nitsche, C. Cordeiro, A. B. Flores, E. W. Knightly, E. Perahia, and J. C. Widmer, "IEEE 802.11ad: Directional 60 GHz communication for multi-gigabit-per-second Wi-Fi," *IEEE Commun. Mag.*, vol. 52, no. 12, pp. 132–141, Dec. 2014.

[21] T. Baykas *et al.*, "IEEE 802.15.3c: The first IEEE wireless standard for data rates over 1 Gb/s," *IEEE Commun. Mag.*, vol. 49, no. 7, pp. 114–121, Jul. 2011.

[22] A. Maltsev, A. Pudeyev, A. Lomayev, and I. Bolotin, "Channel modeling in the next generation mmWave Wi-Fi: IEEE 802.11ay standard," in *Proc. 22nd Eur. Wireless Conf.*, May 2016, pp. 1–8.

[23] *TP Link WiGig Router*. Accessed: Sep. 18, 2017. [Online]. Available: http://static.tp-link.com/AD7200_V2_User%20Guide.pdf

[24] *Netgear WiGig Router*. Accessed: Sep. 18, 2017. [Online]. Available: https://www.netgear.com/images/datasheet/networking/wifirouter/R9000.pdf

[25] *Dell Latitude*. Accessed: Sep. 18, 2017. [Online]. Available: https://www.dell.com/en-us/work/shop/dell-laptops-and-notebooks/latitude-5414/spd/latitude-14-5414-laptop/xctol541414us

[26] *EK1HMC6350 RF Front-End*. Accessed: Sep. 18, 2017. [Online]. Available: http://www.analog.com/media/en/technical-documentation/user-guides/EK1HMC6350-UG-1031.pdf

[27] *PEM009 RF Front-End*. Accessed: Sep. 18, 2017. [Online]. Available: https://www.pasternack.com/images/ProductPDF/PEM009-KIT.pdf

[28] C. Ribeiro and A. Gameiro, "A software-defined radio FPGA implementation of OFDM-based PHY transceiver for 5G," *Analog Integr. Circuits Signal Process.*, vol. 91, no. 2, pp. 343–351, May 2017, 10.1007/s10470-017-0939-x.

[29] P. Zetterberg and R. Fardi, "Open source SDR frontend and measurements for 60-GHz wireless experimentation," *IEEE Access*, vol. 3, pp. 445–456, 2015.

[30] T. Wei and X. Zhang, "mTrack: High-precision passive tracking using millimeter wave radios," in *Proc. 21st Annu. Int. Conf. Mobile Comput. Netw. (MobiCom)*, New York, NY, USA, 2015, pp. 117–129, doi: 10.1145/2789168.2790113.

[31] Y. Zeng, P. H. Pathak, Z. Yang, and P. Mohapatra, "Human tracking and activity monitoring using 60 GHz mmWave: poster abstract," in *Proc. 15th ACM/IEEE Int. Conf. Inf. Process. Sensor Netw. (IPSN)*, Apr. 2016, pp. 1–2.

[32] A. Olivier, "Design, simulation and experimental evaluation of indoor localization schemes for 60 GHz millimeter wave systems," M.S. thesis, Dept. Inf. Eng., Univ. Padua, Padua, Italy, 2015.

[33] Y. Ghasempour and E. W. Knightly, "Decoupling beam steering and user selection for scaling multi-user 60 GHz WLANs," in *Proc. 18th ACM Int. Symp. Mobile Ad Hoc Netw. Comput. (Mobihoc)*, New York, NY, USA, 2017, pp. 10:1–10:10, doi: 10.1145/3084041.3084050.

[34] R. Foster *et al.*, "Beam-steering performance of flat Luneburg lens at 60?GHz for future wireless communications," *Int. J. Antennas Propag.*, vol. 2017, Aug. 2017, Art. no. 7932434, doi: 10.1155/2017/7932434.

[35] T. Nitsche, G. Bielsa, I. Tejado, A. Loch, and J. Widmer, "Boon and bane of 60 GHz networks: Practical insights into beamforming, interference, and frame level operation," in *Proc. 11th ACM Conf. Emerg. Netw. Exp. Technol. (CoNEXT)*, New York, NY, USA, 2015, pp. 17:1–17:13, doi: 10.1145/2716281.2836102.

[36] T. S. Rappaport, Y. Xing, G. R. MacCartney, A. F. Molisch, E. Mellios, and J. Zhang, "Overview of millimeter wave communications for fifth-generation (5G) wireless networks—With a focus on propagation models," *IEEE Trans. Antennas Propag.*, vol. 65, no. 12, pp. 6213–6230, Dec. 2017.

[37] *IEEE Standard for High Data Rate Wireless Multi-Media Networks*, IEEE Standard 802.15.3-2016 (Revision IEEE Std 802.15.3-2003), Jul. 2016, pp. 1–510.

[38] M. Shafi *et al.*, "5G: A tutorial overview of standards, trials, challenges, deployment, and practice," *IEEE J. Sel. Areas Commun.*, vol. 35, no. 6, pp. 1201–1221, Jun. 2017.

[39] T. Obara, T. Okuyama, Y. Aoki, S. Suyama, J. Lee, and Y. Okumura, "Indoor and outdoor experimental trials in 28-GHz band for 5G wireless communication systems," in *Proc. IEEE Annu. Int. Symp. Pers. Indoor, Mobile Radio Commun. (PIMRC)*, Aug. 2015, pp. 846–850.

[40] J. Mashino, K. Satoh, S. Suyama, Y. Inoue, and Y. Okumura, "5G experimental trial of 28 GHz band super wideband transmission using beam tracking in super high mobility environment," in *Proc. IEEE 85th Veh. Technol. Conf. (VTC Spring)*, Jun. 2017, pp. 1–5.

[41] M. Sung, S.-H. Cho, J. Kim, J. K. Lee, J. H. Lee, and H. S. Chung, "Demonstration of IFoF-based mobile Fronthaul in 5G prototype with 28-GHz millimeter wave," *J. Lightw. Technol.*, vol. 36, no. 2, pp. 601–609, Jan. 15, 2018.

[42] "Final radio interface concepts and evaluations for mm-wave mobile communications D4.2," in *Proc. mmMAGIC*, vol. 1, Jun. 2017, pp. 1–180.

[43] S. Parkvall, E. Dahlman, A. Furuskar, and M. Frenne, "NR: The new 5G radio access technology," *IEEE Commun. Standards Mag.*, vol. 1, no. 4, pp. 24–30, Dec. 2017.

[44] D. Shin, S. Suyama, H. Suzuki, and K. Fukawa, "10 Gbps millimeter-wave OFDM experimental system with iterative phase noise compensation," in *Proc. IEEE Radio Wireless Symp.*, Jan. 2013, pp. 184–186.

[45] J. Zhang, X. Zhang, P. Kulkarni, and P. Ramanathan, "OpenMili: A 60 GHz software radio with a programmable phased-array antenna: Demo," in *Proc. 22nd Annu. Int. Conf. Mobile Comput. Netw. (MobiCom)*, New York, NY, USA, 2016, pp. 485–486, doi: 10.1145/2973750.2985614.

[46] G. Yue *et al.*, "Demonstration of 60 GHz millimeter-wave short-range wireless communication system at 3.5 Gbps over 5 m range," *Sci. China Inf. Sci.*, vol. 60, no. 8, p. 080306, Aug. 2017.

[47] "mmWave access and backhaul link tests and presentation of final demonstrator D6.5," in *Proc. MiWaveS*, vol. 1, Jun. 2017, pp. 1–105.

[48] D. Cvetkovski, E. Grass, T. Hälsig, and B. Lankl, "Hardware-in-the-loop demonstration of a 60 GHz line-of-sight 2×2 MIMO link," in *Proc. IEEE 17th Int. Conf. Smart Technol. (EUROCON)*, Jul. 2017, pp. 631–636.

[49] K. Sobaihi, A. Hammoudeh, and D. Scammell, "64.8 GHz wireless personal area network characterisation using single-carrier frequency domain equalisation for indoor channels," *IET Microw., Antennas Propag.*, vol. 7, no. 8, pp. 635–643, Jun. 2013.

[50] Y. Inoue, Y. Kishiyama, S. Suyama, J. Kepler, M. Cudak, and Y. Okumura, "Field experiments on 5G mmW radio access with beam tracking in small cell environments," in *Proc. IEEE Globecom Workshops (GC Wkshps)*, Dec. 2015, pp. 1–6.

[51] *FMC Cards*. Accessed: Sep. 18, 2017. [Online]. Available: https://www.xilinx.com/products/boards-and-kits/fmc-cards.html

[52] *PEM009 TX Board*. Accessed: Sep. 18, 2017. [Online]. Available: https://www.pasternack.com/images/ProductPDF/PEM010.pdf

[53] A. Tarighat, R. Bagheri, and A. H. Sayed, "Compensation schemes and performance analysis of IQ imbalances in OFDM receivers," *IEEE Trans. Signal Process.*, vol. 53, no. 8, pp. 3257–3268, Aug. 2005.

[54] L. Verma, M. Fakharzadeh, and S. Choi, "WiFi on steroids: 802.11AC and 802.11AD," *IEEE Wireless Commun.*, vol. 20, no. 6, pp. 30–35, Dec. 2013.

[55] H. A. Mahmoud and H. Arslan, "Error vector magnitude to SNR conversion for nondata-aided receivers," *IEEE Trans. Wireless Commun.*, vol. 8, no. 5, pp. 2694–2704, May 2009.

[56] N. J. Kasdin, "Discrete simulation of colored noise and stochastic processes and $1/f^\alpha$ power law noise generation," *Proc. IEEE*, vol. 83, no. 5, pp. 802–827, May 1995.

[57] R. Gomes, A. Hammoudeh, R. F. Caldeirinha, Z. Al-Daher, T. Fernandes, and J. Reis, "Towards 5G: Performance evaluation of 60 GHz UWB OFDM communications under both channel and RF impairments," *Phys. Commun.*, vol. 25, pp. 527–538, Dec. 2017. [Online]. Available: http://www.sciencedirect.com/science/article/pii/S1874490717301775

RODOLFO GOMES (S'15) was born in Leiria, Portugal, in 1991. He received the B.Sc. degree in electrical engineering, electronics, and telecommunications from the School of Technology and Management, Polytechnic Institute of Leiria, Leiria, in 2012. He is currently pursuing the Ph.D. degree in electrical engineering with the University of South Wales, Treforest, U.K. He is currently a Researcher with the Antennas and Propagation Research Group, Instituto de Telecomunicações, Leiria. His research interests include the design and implementation of an mm-wave wireless radio system prototype for gigabit/sec multimedia applications and radio wave propagation.

LUÍS SISMEIRO (S'16) was born in Leiria, Portugal, in 1993. He received the B.Sc. degree in electrical engineering, electronics, and telecommunications from the School of Technology and Management, Polytechnic Institute of Leiria, Leiria, in 2015, where he is currently pursuing the M.Sc. degree in electrical engineering. He is currently a Researcher with the Universidad de Vigo, Spain. His research interests include the design of mm-wave wireless systems and energy harvesting from radio-frequency signals.

R. Gomes *et al.*: Will COTS RF Front-Ends Really Cope With 5G Requirements at mmWave?

IEEE *Access*

CARLOS RIBEIRO received the B.Sc. degree in electrical engineering and the M.Sc. degree in electrical and computer engineering from the University of Coimbra, Portugal, in 1996 and 2003, respectively, and the Ph.D. degree in electrical engineering from the University of Aveiro, Portugal, in 2010. He joined the Department of Electronics, Polytechnic Institute of Leiria, Portugal, in 1997, where he is currently an Assistant Professor. He is currently a Researcher in wireless communications with the Antennas and Propagation research Group, Instituto de Telecomunicações, Portugal. His main research topics are PHY algorithms for radio frequency and visible light communication systems, and its implementation. He has published tens of papers in international journals and conferences and has participated in several national and European projects.

AKRAM HAMMOUDEH has extensive practical experience in developing and implementing strategies relating to national and overseas collaboration, student recruitment, and student retention. He supervised and actively engaged in the supervision of a number of Ph.D. students. He is the Founder and the Director of the University of South Wales Branch, Dubai. Before relocating to Dubai, he held a number of senior management positions with the University of South Wales home campus in the U.K. and served as an external examiner for a number of U.K. and overseas HE institutions. He has published over 50 research papers. He is a fellow of the Institute of Engineering and Technology and an active member of the Academic Accreditation Committee.

TELMO R. FERNANDES (S'05–M'06) received the Licenciatura degree in electrical engineering, telecommunications, and electronics, and the M.Sc. degree in channel assignment on cellular networks using neural networks and genetic algorithms from the Faculty of Sciences and Technology, University of Coimbra, Portugal, in 1996 and 2000, respectively, the Ph.D. degree in radio communication systems from the University of Glamorgan, Pontypridd, U.K., in 2007, for his research program in radio wave propagation through vegetation. In 1997, he joined the School of Technology and Management, Polytechnic Institute of Leiria, Leiria, where he is currently a Senior Lecturer. He is currently a Researcher with the Instituto de Telecomunicações, Leiria, Portugal.

RAFAEL F. S. CALDEIRINHA (M'00–SM'15) was born in Leiria, Portugal, in 1974. He received the B.Eng. degree (Hons.) in electronic and communication engineering and the Ph.D. degree in radio wave propagation, with a focus on vegetation studies at frequencies from 1 to 62.4 GHz, from the University of Glamorgan, U.K., in 1997 and 2001, respectively. He is currently the Head of the Antennas and Propagation Research Group, Instituto de Telecomunicações, Leiria, and a Coordinator Professor in mobile communications with the School of Technology and Management (ESTG), Polytechnic Institute of Leiria, Portugal.

His research interests include studies of radio wave propagation through vegetation media, radio channel sounding and modeling, and frequency selective surfaces for applications at microwave and millimeter wave frequencies.

He has authored or co-authored over 120 papers in conferences and international journals and four contributions to the ITU-R Study Group, which formed the basis of the ITU-R P.833-5 (2005) recommendation. He is a fellow and a member of IET. He has been the Regional Delegate of the European Association for Antennas and Propagation for Andorra, Portugal, and Spain, since 2017. He was an Appointed Officer for Awards and Recognitions of the IEEE Portugal Section in 2014. He was the Program Chair of the WINSYS International Conference from 2006 to 2012. He has been the Chair of the IEEE Portugal Joint Chapter on Antennas and Propagation—Electron Devices and Microwave Theory and Techniques since 2016. He is a member of the Editorial Board of the *International Journal of Communication Systems*, (New York, Wiley). He is an Associate Editor of the IEEE TRANSACTIONS ON ANTENNAS and PROPAGATION journal and the *IET on Microwaves, Antennas and Propagation* journal.

MANUEL GARCIA SANCHÉZ (S'88–M'93) received the Ingeniero de Telecomunicación degree from the Universidad de Santiago de Compostela, Spain, in 1990, and the Doctor Ingeniero de Telecomunicación (Ph.D.) degree from the Universidad de Vigo, Spain, in 1996. His research interests include studies of indoor and outdoor radio channel sounding and modeling for narrow and wide-band applications at microwave and millimeter wave frequencies, point-to-multipoint radio links, mobile communications, UMTS, WLANs, and DVB-T distribution networks.

• • •